

Novel constraints on neutrino physics beyond the standard model from the CONUS experiment

CONUS Collaboration

H. Bonet,^a A. Bonhomme ^a, C. Buck ^a, K. Fülber,^b J. Hakenmüller ^a, G. Heusser,^a T. Hugle ^a, M. Lindner ^a, W. Maneschg ^a, T. Rink ^a, H. Strecker^a and R. Wink^b

^aMax-Planck-Institut für Kernphysik, Saupfercheckweg 1, 69117 Heidelberg, Germany

^bPreussenElektra GmbH, Kernkraftwerk Brokdorf, Osterende, 25576 Brokdorf, Germany

E-mail: conus.eb@mpi-hd.mpg.de

ABSTRACT: The measurements of coherent elastic neutrino-nucleus scattering ($\text{CE}\nu\text{NS}$) experiments have opened up the possibility to constrain neutrino physics beyond the standard model of elementary particle physics. Furthermore, by considering neutrino-electron scattering in the keV-energy region, it is possible to set additional limits on new physics processes. Here, we present constraints that are derived from CONUS germanium data on beyond the standard model (BSM) processes like tensor and vector non-standard interactions (NSIs) in the neutrino-quark sector, as well as light vector and scalar mediators. Thanks to the realized low background levels in the CONUS experiment at ionization energies below 1 keV, we are able to set the world's best limits on tensor NSIs from $\text{CE}\nu\text{NS}$ and constrain the scale of corresponding new physics to lie above 360 GeV. For vector NSIs, the derived limits strongly depend on the assumed ionization quenching factor within the detector material, since small quenching factors largely suppress potential signals for both, the expected standard model $\text{CE}\nu\text{NS}$ process and the vector NSIs. Furthermore, competitive limits on scalar and vector mediators are obtained from the $\text{CE}\nu\text{NS}$ channel at reactor-site which allow to probe coupling constants as low as $5 \cdot 10^{-5}$ of low mediator masses, assuming the currently favored quenching factor regime. The consideration of neutrino-electron scatterings allows to set even stronger constraints for mediator masses below ~ 1 MeV and ~ 10 MeV for scalar and vector mediators, respectively.

Contents

1	Introduction	1
2	Data sets, experimental framework and analysis method	3
2.1	Data sets and the experimental framework of the CONUS experiment	3
2.2	Standard model expectation, likelihood function and systematic uncertainties	7
3	Constraints on beyond the standard model neutrino physics	10
3.1	Non-standard interactions	11
3.1.1	Tensor-type interaction	13
3.1.2	Vector-type interaction	15
3.2	Simplified mediator models	17
3.2.1	Light vector bosons	17
3.2.2	Light scalar bosons	22
4	Conclusions	23

1 Introduction

Coherent elastic neutrino-nucleus scattering ($\text{CE}\nu\text{NS}$) is a standard model (SM) process of elementary particle physics that was predicted shortly after the discovery of the Z -boson [1–3]. After over forty years, first observations of this process were reported by the COHERENT Collaboration, using a pion-decay-at-rest (πDAR) source in combination with scintillation and liquid noble gas detectors [4, 5]. The CONUS experiment pursues detecting this interaction channel with reactor electron antineutrinos and recently published first limits [6]. The underlying data were acquired with low background germanium detectors located at 17.1 m distance from the reactor core center of the 3.9 GW (thermal power) nuclear power plant in Brokdorf, Germany.

So far, no deviations from the SM prediction have been observed in the operational experiments. However, new possibilities to search for physics beyond the standard model (BSM) have already triggered various phenomenological investigations [7–10]. Together with their expected SM interactions, any new interaction of neutrinos can play an important role in a wide range of physics branches: from cosmology to the smallest scales of nuclear and particle physics. In an astronomical context, they play a key role in the evolution of stellar collapses [11, 12] and might influence stellar nucleosynthesis [13]. In addition, with neutrino detection via $\text{CE}\nu\text{NS}$ at hand, flavor-independent astronomy with supernova neutrinos becomes feasible [14–16] and thus allows to investigate the interior of dense objects as well as stellar evolution in detail. The next-generation dark matter direct-detection experiments will face an irreducible background, the so-called neutrino-floor, which is caused

by atmospheric, solar and supernova remnant neutrinos that coherently scatter in such detectors [17, 18]. From the perspective of neutrino physics, this opens up new possibilities as new neutrino interactions might manifest themselves in this “background” as well [19–23].

In a nuclear and particle physics context, even without any new physics contributions, CE ν NS can allow for a determination of the neutron density distribution of a target nucleus [24–27] as well as the weak mixing angle in the unexplored MeV regime [28–31].

For BSM searches, CE ν NS detectors can be used to search for non-standard neutrino-quark interactions (NSIs) [32–41] and to investigate potential electromagnetic properties of the neutrino [42–46], e.g. finite magnetic moments or a millicharge. Being at lower energy scales than typical collider experiments, CE ν NS experiments complement their BSM searches and might result in either competitive or even stronger bounds for light mediators [47, 48]. In particular, investigations of light scalars and/or axion-like particles [49–51], and light vectors [52–55], e.g. dark photons, take advantage of this new channel. Even searches for new fermions seem possible within the context of CE ν NS measurements [56, 57].

More generally, a high statistics CE ν NS measurement can be used to determine the flux of a neutrino source precisely. Regarding the flux anomalies reported from several short-baseline experiments and the possible eV-mass sterile neutrino solution [58–60], CE ν NS might contribute further knowledge, especially since it provides flavor-blind and energy-threshold-free information about the source’s (anti)neutrino spectrum [61–65]. Particularly at nuclear reactors, small (and therefore simpler to integrate) CE ν NS sensitive devices could help in monitoring their power and flux and, in the future, even determine a reactor’s antineutrino spectrum below 1.8 MeV, which is usually limited by the threshold energy of the used detection channel, i.e. inverse beta-decay (IBD). In this way, neutrino physics might help in reactor safeguarding and contribute to nuclear non-proliferation [66–68].

All the above mentioned SM and BSM possibilities in combination with improvements in detector and background suppression techniques have made CE ν NS measurements a feasible and promising endeavor both at neutrino π DAR sources and nuclear reactors. While the COHERENT Collaboration is preparing the operation of further detector systems with different target elements at a π DAR neutrino source, there are many more experimental attempts to measure CE ν NS with electron antineutrinos emitted from nuclear reactors: CONNIE [69], MINER [70], NCC-1701 at DRESDEN-II [71], NEON [72], ν -cleus [73], ν GEN [74], RED-100 [75], RICOCHET [76] and TEXONO [77]. In these reactor experiments, different detection technologies are used, e.g. charged-coupled devices (CCDs) [78], cryogenic calorimeters [79], high-purity germanium (HPGe) crystals [80], liquid noble gas detectors [81] as well as scintillating crystals [82]. In this way, the field of CE ν NS is going to be probed with the full range of recent detector technologies and different target nuclei – each with its own particular advantages and complementarities – allowing to expect interesting results from SM as well as BSM investigations.

As a part of the experimental efforts in this direction, we present here the first BSM results derived from the CONUS RUN-1 data. We use a very similar analysis procedure to the one employed for the experiment’s first CE ν NS limit determination [6] and apply it to common BSM models that have already been investigated in the context of other CE ν NS measurements. In particular, we show bounds on tensor and vector NSIs as well as

simplified light vector and scalar mediator models. For the latter two, we deduce bounds from neutrino scattering off electrons and off nuclei.

This paper is structured as follows: In Section 2 we describe the analysis method that is used for the BSM models in the course of this paper. Next to a general introduction of the CONUS set-up, we give an overview of the analysis procedure as well as systematic uncertainties that underlie this investigation. We further introduce two data sets that are chosen for the two scattering channels under study, i.e. neutrino-nucleus and neutrino-electron scattering. Subsequently, we show the results of the performed investigations in Section 3. Limits on tensor and vector NSIs are presented and in the context of light vector and scalar mediator searches, we derive bounds from electron scattering in the ionization energy region between 2 and 8 keV_{ee}.¹ Finally, in Section 4 we conclude and give an outlook on the various BSM investigations that will become feasible with CONUS and the next generation of CE ν NS experiments.

2 Data sets, experimental framework and analysis method

For the analysis presented here, we use the CONUS RUN-1 data and employ a binned likelihood analysis to derive limits on parameters of the considered BSM models. In addition to the RUN-1 data set used for the CE ν NS analysis described in Ref. [6], we work with a second RUN-1 data set at energies between 2 and 8 keV_{ee}, which exhibits longer data collection periods for the BSM channels that are sensitive to neutrino-electron scattering. The details of both data sets as well as the likelihood analysis are laid out in the following subsections.

2.1 Data sets and the experimental framework of the CONUS experiment

The data sets used in this BSM analysis were gathered during RUN-1 (Apr 01 - Oct 29, 2018) of the CONUS experiment which is operated at the commercial nuclear power plant in Brokdorf, Germany. Inside the nuclear power plant is a single-unit pressurized water reactor that is operated at a maximal thermal power of 3.9 GW and serves as an intense electron antineutrino source at the 17m-distant experimental site. The expected antineutrino spectrum is a typical reactor spectrum, dominated by the contribution of the four isotopes ²³⁵U, ²³⁸U, ²³⁹Pu and ²⁴¹Pu [83], with all of the neutrinos having energies of less than ~ 10 MeV. To describe the antineutrino emission spectrum from the reactor, we start from the predicted antineutrino spectra by Huber and Müller [84, 85] and correct for the 5 MeV-bump observed in experimental data [86]. The relative contribution of the different isotopes can be accounted for by weighting the different isotopes according to their time-dependent fission fractions, which are provided to us by the reactor operating company PreussenElektra GmbH. The corresponding values for the three detectors CONUS-1, CONUS-2 and CONUS-3 (C1-C3) considered in the following analyses are listed in Table 1. This reactor spectrum above the 1.8 MeV threshold of IBD experiments determines the neutrino

¹The notations “eV_{ee}” and “eV_{nr}”, will be used in the following as a shorthand notation to distinguish ionization energy, denoted as *ee* (as a reference to “electron equivalents”), and nuclear recoil energy, denoted as *nr*.

Detector	^{235}U [%]	^{238}U [%]	^{239}Pu [%]	^{241}Pu [%]	\bar{P}_{th} [%]
C1	60.3; 56.8	7.1; 7.2	27.0; 29.9	5.4; 6.1	92.33; 89.88
C2	63.8; 56.9	7.1; 7.2	24.2; 29.8	4.9; 6.1	92.70; 90.12
C3	57.2; 56.8	7.2; 7.2	29.7; 29.9	6.0; 6.1	88.79; 90.10

Table 1. Average fission fractions of the most relevant isotopes in the reactor antineutrino spectrum and average reactor powers \bar{P}_{th} in terms of the reactor’s maximal thermal power of 3.9 GW for standard/extended data sets of CONUS RUN-1. The detectors C1-C3 used in the following analyses are assigned individual values due to their specific data collection periods.

spectrum for all processes associated with nucleus scattering. For the electron scattering channels that we analyze, also the low-energy part (below 1.8 MeV) of the spectrum becomes relevant for which we use the simulation data provided by Ref. [87]. These simulations for the different isotopes can be weighted by the fission fractions and normalized to the total number of neutrinos emitted over the whole spectrum, of which there are on average ~ 7.2 per fission, cf. Ref. [88]. To determine the total flux of antineutrinos that can interact with the CONUS detectors, we can use the total number of fissions per second derived from the reactor thermal power, as every fission releases about 200 MeV of energy (cf. Ref. [89] for details and exact isotope specific values). This leads to a total antineutrino flux at the experimental site of $2.3 \cdot 10^{13} \text{ s}^{-1} \text{ cm}^{-2}$. The influence of the shape uncertainties, i.e. the covariance matrix of the neutrino spectrum as provided by Ref. [86], was investigated in the context of the CONUS CE ν NS analysis [6] and turned out to be negligible in our case. Therefore, we do not include them in the present analysis.

Besides the immense reactor flux and the corresponding spectral distribution of antineutrinos, the achieved background level with the deployed shield is another cornerstone of the whole experimental framework. The shield is extremely compact, with a volume of only 1.65 m³ and a mass of 11 tonnes, and exhibits an onion-like structure. It consists of lead bricks, borated and non-borated polyethylene plates, and plastic scintillator plates equipped with photomultiplier tubes serving as an active muon anticoincidence system (muon veto). Around the layers, a protective stainless steel cage helps fulfilling the safety requirements. The shield design is based on the long-time experience with low background techniques at Max-Planck-Institut für Kernphysik (MPIK), e.g. Refs. [90, 91], while being optimized to the experimental site at shallow depth next to a reactor core. The location of the CONUS detector and the dimension of the whole set-up within the nuclear power plant are illustrated in Figure 1.

The influence of possible reactor-correlated background types was confirmed to be negligible via dedicated neutron and γ -ray measurement campaigns. These were supported by validated background Monte Carlo (MC) simulations that incorporated a large fraction of the reactor geometry surrounding the experimental site [92]. Thus, the background to the BSM analyses is uncorrelated to the reactor thermal power. It is described like in the CE ν NS investigation by MC simulations. For the BSM analyses of both scattering channels, the

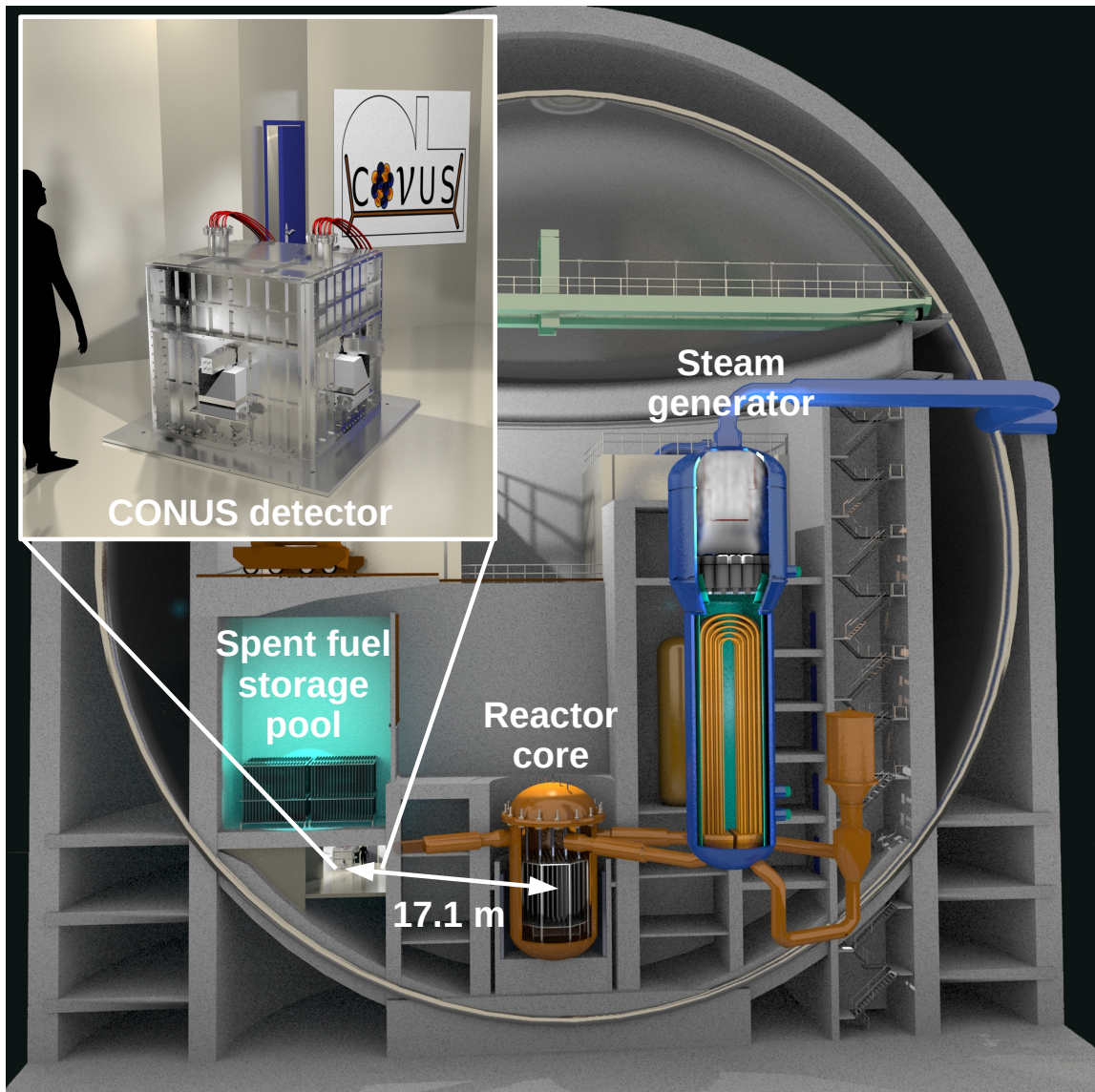


Figure 1. Position of the CONUS detector set-up within the building of the nuclear power plant at Brokdorf, Germany. It is located under the spent fuel storage pool at 17.1 m distance to the 3.9 GW (thermal power) reactor core. The vertical position of the set-up coincides approximately with the reactor core's center. The enlarged image shows the set-up at its experimental site. Within the shown stainless steel cage, layers of lead as well as pure and borated polyethylen serve as passive shield around the embedded four HPGe detectors against external radiation and other background sources. Further, it includes plastic scintillator plates equipped with photomultiplier tubes which are used as muon veto.

background model is almost identical to the one used in the CE ν NS publication, cf. Ref. [6]. Only small adjustments to the background model have been made for the extended data sets, which are used for the electron scattering channels. In that context due to the extended region of interest (ROI) to higher energies, systematic uncertainties on the spectral shape of the background model are considered in order to account for uncertainties regarding the production rate of cosmogenic induced isotopes as well as surface contamination on the Ge diodes. Details of the applied background model and its uncertainties can be found in a dedicated background description of the CONUS experiment, cf. Ref. [93]. In the energy window of 500 to 1000 eV $_{ee}$, just above the ROI for CE ν NS studies, the CONUS detectors achieve background levels of a few 10 counts kg $^{-1}$ d $^{-1}$ keV $_{ee}^{-1}$, while having an effective overburden of 24 m of water-equivalent (m w.e.) only.

To detect the antineutrinos that cross the shield, CONUS uses four 1 kg-sized point-contact HPGe spectrometers with sub-keV $_{ee}$ energy thresholds. A full description can be found in Ref. [80]. The four detectors have a total active mass of (3.73 ± 0.02) kg and provide the necessary characteristics for a CE ν NS measurement at a commercial reactor site: ultra-low noise levels and thus very low energy thresholds, i.e. $\lesssim 300$ eV $_{ee}$, low concentrations of radioactive contamination as well as electrically powered cryocoolers. Within a CE ν NS process, the induced nuclear recoil releases heat and ionization electrons that might be collected by an appropriate detector for signal formation. However, in the present case, only the ionization energy part is registered by the HPGe detectors, resulting in an energy that is suppressed by 75 – 85% compared to the original recoil energy. This phenomenon is commonly referred to as ‘quenching’. Consequently, this makes detecting CE ν NS signals even more difficult. To take the effect of quenching into account, we apply the widely used Lindhard model [94], modified with an adiabatic correction [95]. Its associated parameter k roughly corresponds to the quenching factor at nuclear recoils of ~ 1 keV $_{nr}$. One recent measurement indicates that quenching deviates from this description especially at ionization energies of ~ 250 eV $_{ee}$ and below, cf. Ref. [96].² Thus, an accurate determination of the quenching factor cannot only support CE ν NS measurements, but also affects BSM studies [98] as it appears in any process that involves scattering off a nucleus. So far, there is a variety of measurements for the quenching factor in germanium with larger systematic uncertainties that still leave enough room to constitute the dominating source of uncertainty for our BSM analyses here. To account for this uncertainty, we always present the results for different quenching factors which cover the range of currently available experimental data.

Generally, the CONUS data acquisition is divided into reactor ON and reactor OFF periods as well as periods reserved for commissioning and optimization. Each data set then has been defined individually according to the stability of environmental parameters like ambient temperature. For the details of this data selection procedure we refer to Ref. [80]. In the present analysis, we use data of the first acquisition period which we refer to as RUN-1 data set. For this data set, the CONUS-4 (C4) detector is excluded due to a temporarily

²Note that for such low energies, simplifying assumptions underlying the Lindhard model can be questioned and deviations might be described by an additional parameter [97].

Scattering channel	Detector	ON [kg d]	OFF [kg d]	ROI [eV _{ee}]
$\bar{\nu}_e + A(Z, N)$	C1	96.7	13.8	276 - 741
	C2	14.6	13.4	281 - 999
	C3	97.5	10.4	333 - 991
	all	208.8	37.6	
$\bar{\nu}_e + e$	C1	215.4	29.6	2013 - 7968
	C2	184.6	32.2	2006 - 7990
	C3	248.5	31.7	2035 - 7989
	all	648.5	93.5	

Table 2. Lifetimes for reactor ON and OFF periods together with the regions of interest (ROIs) for the different detectors in both scattering channels during RUN-1, specifying the data sets that are investigated for BSM signatures in this work.

appearing artifact, cf. Ref. [6]. Besides neutrino-nucleus scattering, where only the region below 1 keV_{ee} is important, we also analyze neutrino-electron scattering at energies between 2 and 8 keV_{ee}. We limit our analysis of the electron channel to this energy interval because of two reasons: First, we are looking at signals that emerge as broader spectral contribution above the continuum of the spectrum. The selected region is line-free and naturally confined by x-ray peaks around ~ 1 keV and ~ 10 keV, which are due to K- and L-shell transitions in decays of Ge-related isotopes. These isotopes were/are produced by cosmic activation above ground and partially in-situ at the experimental site, as well as via sporadically deployed artificial neutron calibration sources. Second, the new ROI is not affected at all by potential noise, that is correlated with the ambient temperature, cf. Ref. [80], and which caused an exclusion of parts of the data from our first CE ν NS analysis in the sub-keV regime. Thereby, we can increase the total lifetime of the extended data set, compared to the CE ν NS data set, by a factor of 3.1 for ON and a factor of 2.5 for OFF periods. The specifications of all final data sets after data selection and cuts, used for the BSM analysis in this paper, are depicted in Table 2.

2.2 Standard model expectation, likelihood function and systematic uncertainties

The following investigation relies on a similar analysis chain as the CE ν NS investigation in Ref. [6]. In this way, we are able to determine realistic bounds on the individual model parameters, while including all relevant experimental uncertainties. Here we briefly introduce the SM expectations, the performed likelihood procedure and give an overview of the included systematic uncertainties.

The main ingredient of our analysis is a binned likelihood ratio test, cf. Refs. [99–101]. We fix the individual BSM parameters and compare their likelihood value to the one of the null hypothesis, which includes the SM signal of neutrino-nucleus as well as neutrino-electron scattering. Hence, CE ν NS and neutrino-electron scattering are either modified through

interference with new BSM physics or, in the case they are independent, simply appear as an additional background component in the BSM analysis. From a simulation of the corresponding test statistic (toy MC) we extract limits on these model parameters at 90% confidence level (C.L.).

The differential cross section of the SM predicted CE ν NS process is given by, cf. Ref. [1],

$$\frac{d\sigma}{dT_A}(T_A, E_\nu) = \frac{G_F^2}{\pi} \mathcal{Q}_W^2 m_A \left(1 - \frac{m_A T_A}{2E_\nu^2}\right) F^2(T_A), \quad (2.1)$$

with the nuclear recoil energy T_A , Fermi's constant G_F , the nuclear mass m_A and the neutrino energy E_ν . We use the nuclear charge³

$$\mathcal{Q}_W = g_V^p Z + g_V^n N = \left(\frac{1}{2} - 2\sin^2\theta_W\right) Z - \frac{1}{2}N, \quad (2.2)$$

with the Weinberg angle θ_W , the number of protons Z and the number of neutrons N in the target nucleus, respectively. Further, the nuclear form factor $F(T_A)$ describes the degree of deviation from scattering off a point-like object. It is approximated with unity for the rest of this analysis which is justified by the small momentum transfer of reactor antineutrinos. Thus, at a reactor-site the interaction of antineutrinos with the target nuclei can be seen as a process in the fully coherent regime. At higher energies, i.e. at π DAR sources, the loss of coherent enhancement is usually described via the form factor parameterization by Helm [102] or by Klein and Nystrand [103]. However, the decrease in cross section is small, i.e. a factor of ~ 1.4 for the COHERENT experiment [104], and introduces only minor uncertainties of $\lesssim 5\%$ [4, 105].

Though the (anti)neutrino-electron scattering process $\bar{\nu}_e e^- \rightarrow \bar{\nu}_e e^-$ contributes only as a small background to the CE ν NS ROI, it is relevant for our analysis of the light mediator electron channels at higher energies. The corresponding SM cross section is found to be, cf. Ref. [106],

$$\frac{d\sigma}{dT_e}(T_e, E_\nu) = \frac{G_F^2 m_e}{2\pi} \left[(g_V + g_A)^2 + (g_V - g_A)^2 \left(1 - \frac{T_e}{E_\nu}\right) + (g_A^2 - g_V^2) \frac{m_e T_e}{E_\nu^2} \right]. \quad (2.3)$$

Herein, T_e stands for the electron recoil, and $g_V = \frac{1}{2} + 2\sin^2\theta_W$ and $g_A = -\frac{1}{2}$ for the effective vector and axial-vector couplings, respectively.⁴ In the case of neutrino-electron scattering, atomic binding effects for recoil energies comparable to atomic binding energies have to be taken into account. We follow the procedure proposed in Ref. [107] and apply electron binding energies of germanium taken from Ref. [108].

³Sometimes, the weak nuclear charge is defined as $\mathcal{Q}_W = (1 - 4\sin^2\theta_W)Z - N$ such that the prefactor of Eq. (2.1) includes an additional factor of $\frac{1}{4}$.

⁴Generally, the vector and axial-vector couplings to the Z boson are defined as $g_V^f = I_3^f - 2q^f \sin^2\theta_W$ and $g_A^f = I_3^f$, respectively. For example, in the case of a muon one obtains $g_V^\mu = -\frac{1}{2} + 2\sin^2\theta_W$ and $g_A^\mu = -\frac{1}{2}$ which reflects a pure neutral current interaction. In case of an electron, there is an additional W boson exchange that enhances the couplings, i.e. $g_{V,A} \rightarrow g_{V,A} + 1$. For antineutrinos, the charged current is mediated via a s-channel diagram (instead of a t-channel), which further leads to $g_A \rightarrow -g_A$.

Both interaction channels exhibit a maximum recoil energy obtained from pure forward scattering,

$$T_x^{\max} = \frac{2E_\nu^2}{m_x + 2E_\nu} \quad \text{for } x = \{e, A\}. \quad (2.4)$$

Note that electron recoils are, contrary to CE ν NS, not affected by quenching, and, thus, the maximal detectable energy, i.e. recoil energy subtracted by the electron’s binding energy, lies far above the analyzed ROIs. For antineutrinos emitted from a reactor core, i.e. $E_\nu \sim 10$ MeV, we obtain maximal recoil energies of ~ 9.9 MeV and ~ 3.0 keV for electrons and germanium nuclei, respectively. As a result, SM neutrino-electron scattering features a flat contribution in our ROI whereas the CE ν NS signal rises towards lower energies with a shift in energy according to the underlying quenching factor.

Both cross sections have to be convolved with the reactor antineutrino spectrum $\frac{dN}{dE_\nu}$, such that the final number of events is given by

$$N_x^{\text{SM}} = t \cdot \Phi^* \cdot N_x^{\text{Ge}} \sum_i^{N_{\text{bins}}} \int_{T_i - 0.5\Delta T}^{T_i + 0.5\Delta T} dT \int_{E_{\text{min}}}^{E_{\text{max}}} dE_\nu \frac{dN}{dE_\nu}(E_\nu) \left(\frac{d\sigma}{dT} \right)_x(T, E_\nu) \quad (2.5)$$

with the experimental lifetime t , N_x^{Ge} for $x = \{e, A\}$ as the number of target electrons and nuclei respectively, N_{bins} the number of spectral bins and T_i the energy at the bin center with the bin width ΔT . The ‘reduced’ reactor flux incorporates all reactor-related quantities and is given by

$$\Phi^* = \frac{P_{\text{th}}}{4\pi d^2 \bar{E}}, \quad (2.6)$$

with the thermal reactor power P_{th} , the detector’s distance to the reactor d and the average energy release per fission \bar{E} , cf. Section 2.1. The integral over the applied reactor model yields the number of neutrinos emitted per fission and, multiplied with Φ^* , gives the expected neutrino flux in units of $\text{cm}^{-2} \text{s}^{-1}$ at the experimental site. Special care has to be taken for the conversion of nuclear recoil energy into detectable signal (ionization energy), which depends on dissipation processes in the chosen detector technology and target material. To describe this quenching process in germanium, cf. Section 2.1, we select three representative k -parameter values $k = \{0.12, 0.16, 0.20\}$, i.e. spanning the available measured range in the keV $_{ee}$ regime [95, 96, 109–113]. Thereby we make a substantial uncertainty appearing in our analysis explicit. Finally, the signal expectation has to be convolved with the individual detector response, i.e. the energy resolution and the electronic detection efficiency. For details of the HPGe detectors used within CONUS, we refer to our detector publication [80].

In our likelihood procedure, ON and OFF spectra are fitted simultaneously and additional knowledge on parameters is represented by Gaussian pull terms,

$$-2 \log \mathcal{L} = -2 \log \mathcal{L}_{\text{ON}} - 2 \log \mathcal{L}_{\text{OFF}} + 2 \sum_i \frac{(\Theta_i - \Theta_i^*)^2}{2\sigma_i^2}. \quad (2.7)$$

Herein, the parameters Θ_i of the pull terms have central values Θ_i^* and uncertainties σ_i . The individual detector’s noise edge is fitted with an exponential shape parameterized

by two free parameters, Θ_{thr_1} and Θ_{thr_2} . For the noise edge description, we refined the exponential function used in Ref. [6] and extended the fit range slightly to lower energy thresholds. The MC background model, which will be discussed in detail in a separate publication, cf. Ref. [93], represents the physical background components and appears in the likelihood together with a factor Θ_{b_0} that allows for an overall rescaling as well as two additional uncertainties $\Theta_{b_{1,2}}$ allowing for small variations in the shape of the background model. These additional degrees of freedom are necessary to incorporate the uncertainties on the production rates of cosmogenic induced isotopes as well as on detector surface effects, i.e. from the thickness of the passivation layer. The latter especially influences the spectral shape of the background contributions resulting from decays of contaminants on the diode surface such as ^{210}Pb . The corresponding uncertainties do not exceed 5% and the energy spectrum of the background model is allowed to vary within this range via a second order polynomial distortion. Overall, pull terms are assigned to each detector’s active volume, its electronic detection efficiency c_{eff} , its energy scale calibration uncertainty ΔE and the reduced flux Φ^* . The uncertainty of the reduced neutrino flux $\Delta\Phi^*$ is found to be $\sim 3\%$, depending on the detector and run, and is dominated by the uncertainty on the reactor thermal power ($\Delta P = 2.3\%$) [92], the energy released per fission and isotope (cf. Ref. [89]), as well as the detector’s distance to the reactor core (17.1 ± 0.1) m and correlations among fission fractions (cf. Ref. [86]). Summarizing the parameters related to the reactor model as Θ_{reactor} and the ones related to the detector as Θ_{det} , we can write schematically:

$$\begin{aligned} & -2 \log \mathcal{L}_{\text{ON}}(\Theta_{b_{0,1,2}}, \Theta_{\text{thr}_{1,2}}, \Theta_{\text{reactor}}, \Theta_{\text{det}}, \Theta_{\Delta E}), \\ & -2 \log \mathcal{L}_{\text{OFF}}(\Theta_{b_{0,1,2}}, \Theta_{\text{thr}_{1,2}}, \Theta_{\text{det}}, \Theta_{\Delta E}). \end{aligned} \tag{2.8}$$

In Table 3, we provide an overview of the uncertainties that enter our likelihood procedure and their approximate size. Note that the quenching factor is not quoted with an uncertainty as it is the overall dominating systematics and thus is explicitly taken into account by deriving the limits for different k -values.

The signal hypotheses, which the likelihood compares to the experimental data, are defined by the BSM models described in Section 3. They are implemented through their corresponding cross sections. An exemplary (combined) fit to the collected data is illustrated in Figure 2 for detector C2 and quenching parameter $k = 0.16$ in the case of a light scalar mediator, cf. Section 3.2.2. Contributions to CE ν NS are tested for energies below 1 keV $_{ee}$, while the ones to elastic neutrino-electron scattering are examined within an energy range between 2 and 8 keV $_{ee}$. Further data with their corresponding background models can be found in Refs. [6, 93, 114]. For the minimization of the likelihood we use the iminuit package [115, 116], while the whole analysis is set up within the SciPy framework [117–124]. The extensive cluster computations are done with the help of the software package MPI for Python [125, 126].

3 Constraints on beyond the standard model neutrino physics

After introducing the experimental characteristics and details of the analysis method, we investigate the CONUS RUN-1 data set with respect to BSM signatures and compare

Quantity	Uncertainty or related parameter
background MC	Θ_{b_0} (free), Θ_{b_1, b_2} ($\leq 5\%$, uncertainty from background model)
noise threshold	$\Theta_{\text{thr}_1}, \Theta_{\text{thr}_2}$ (free, uncertainty calculated via toy MC)
reduced neutrino flux $\Delta\Phi^*$	$\sim 3\%$
neutrino spectrum	subdominant uncertainty (compared to quenching)
reactor ON and OFF duration	negligible uncertainty
active mass	$< 1\%$
electronic detection efficiency c_{eff}	$\leq 5\%$
energy calibration uncertainty ΔE	15 eV_{ee}
quenching	k (explicitly included)

Table 3. Overview of the quantities entering the likelihood and their corresponding uncertainties. For details and further information see main text.

our results to limits obtained from other CE ν NS experiments. In particular, we deduce constraints for tensor and vector NSIs as well as simplified light vector and scalar mediators. For the latter cases, we can additionally analyze the electron channels of these models with an extended data set at energies between 2 and 8 keV $_{ee}$.

3.1 Non-standard interactions

A rather model-independent probe of various BSM neutrino physics scenarios are so-called NSIs in the neutrino-quark sector, which are an extension of the neutral current with effective four-fermion operators, generally assuming new mediators that are much heavier than the SM gauge bosons [39]. Since the heavy mediators are conventionally integrated out, the new couplings are defined in terms of Fermi's constant G_F analogously to weak interactions at low energy. In general, these new couplings can be flavor-preserving $\epsilon_{\alpha\alpha}$ and/or flavor-violating $\epsilon_{\alpha\beta}$ with $\alpha \neq \beta$ and $\alpha, \beta = \{e, \mu, \tau\}$ being the lepton flavor indices. Searches of these new neutrino interactions are relevant since they may affect neutrino oscillations [127] and even other physics branches like cosmology [128] or astrophysics [12, 129]. NSIs in their original definition can be studied since they enter the SM CE ν NS cross section via a modified or an additional nuclear charge [32, 33, 35]. More recently, they have been investigated on more general grounds, i.e. in the context of so-called general neutrino interactions (GNIs) [130, 131]. As CONUS operates in the fully coherent regime, the subtleties that can arise for the form factor in BSM models, cf. Ref. [132], are not of relevance to our analysis here.

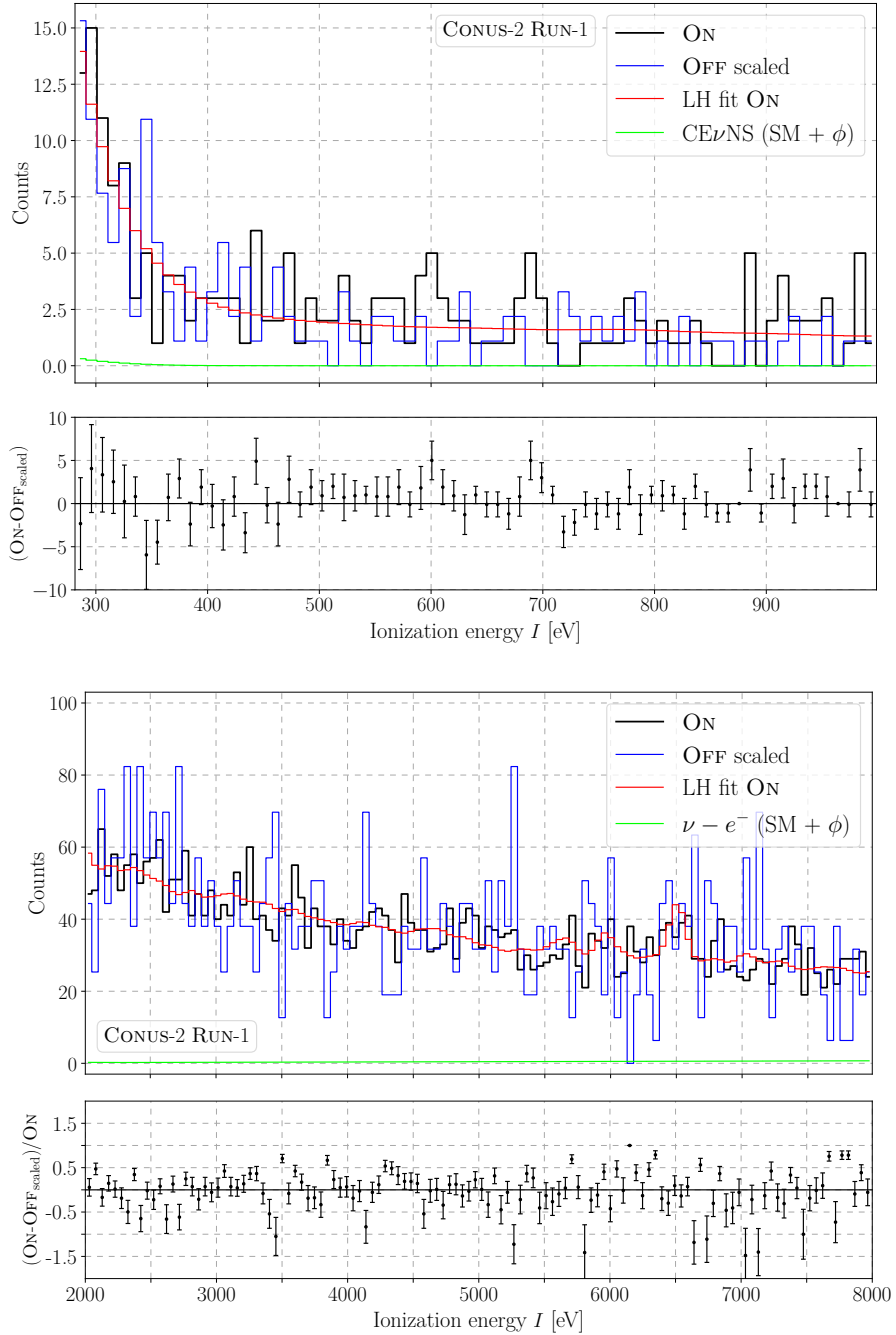


Figure 2. Exemplary fits to experimental data in the case of a simplified light scalar mediator, cf. Section 3.2.2. A combined fit to all data sets of Table 2 is performed and collected reactor ON data (black), the scaled reactor OFF data (blue) as well as the obtained likelihood fit (red) are illustrated for detector C2 and a quenching parameter of $k = 0.16$, assuming free coupling and mediator mass of the underlying BSM model. The received signal events (SM + BSM contribution) are indicated in green. Top: Fit of the modified CE ν NS signal in the ROI below 1 keV_{ee} . To illustrate the agreement between the collected reactor ON and reactor OFF periods, we show the corresponding residuals in total events beneath. Bottom: Fit of modified neutrino-electron scattering in the ROI between 2 and 8 keV_{ee} . To quantify the agreement of reactor OFF data with the collected ON data, residuals are given again (here normalized to the collected ON data).

3.1.1 Tensor-type interaction

Non-standard neutrino-quark interactions of tensor-type can arise in generalizations of the conventional vector NSI approach [34] and naturally occur in the context of GNIs [130, 131]. Furthermore, they might also be associated with electromagnetic properties of neutrinos [133, 134]. Here, we assume the existence of new tensor-type interactions between neutrinos and quarks which are induced by an operator of the form

$$\mathcal{O}_{\alpha\beta}^{qT} = (\bar{\nu}_\alpha \sigma^{\mu\nu} \nu_\beta) (\bar{q} \sigma_{\mu\nu} q) + \text{h.c.}, \quad (3.1)$$

with q denoting the first generation of quarks $q = \{u, d\}$ and $\alpha, \beta = \{e, \mu, \tau\}$ being the lepton flavor indices. Due to a different chiral structure, there is no possibility of destructive interference with the SM channel. The corresponding couplings to quarks can be combined into a new nuclear charge in equivalence to the SM weak charge appearing in the CE ν NS cross section of Eq. (2.1). Thus, in our case we have

$$\mathcal{Q}_{\text{NSI}}^T = \left(2\epsilon_{\alpha\beta}^{uT} + \epsilon_{\alpha\beta}^{dT}\right) Z + \left(\epsilon_{\alpha\beta}^{uT} + 2\epsilon_{\alpha\beta}^{dT}\right) N, \quad (3.2)$$

with the lepton flavor indices α, β as well as Z and N representing the respective number of protons and neutrons in the target nucleus. Note that in contrast to the SM case, cf. Eq. (2.1) and Eq. (2.2), here, as well as in the other BSM models, the proton number does not get weighted with a small prefactor. Thus, the cross section does not necessarily scale with the characteristic dependence on the squared neutron number. Although flavor-changing tensor-type interactions can in principle appear and are for example tested at π DAR sources [7], at reactor site we are only able to probe couplings related to the electron flavor. Therefore, in this analysis, we focus on flavor-diagonal couplings, i.e. ϵ_{ee}^{uT} and ϵ_{ee}^{dT} .

The new tensor-type interaction simply adds to the conventional CE ν NS cross section, resulting in, cf. Ref. [134],

$$\left(\frac{d\sigma}{dT_A}\right) = \left(\frac{d\sigma}{dT_A}\right)_{\text{CE}\nu\text{NS}} + \frac{4G_F^2}{\pi} \mathcal{Q}_{\text{NSI}}^T{}^2 m_N \left(1 - \frac{m_A T_A}{4E_\nu^2}\right). \quad (3.3)$$

Note the different kinematic factors between the CE ν NS cross section in Eq. (2.1) and Eq. (3.3) which allow the tensor NSI signal to extend to higher energies. The upper plot of Figure 3 illustrates the modified signal expectation in detector C1 due to additional tensor NSIs in comparison to the SM case. It shows when up- and down-quark couplings have different signs, the amplitude of the BSM signal is significantly smaller than in the case of same signs.

The obtained limits at 90% C.L. for tensor NSIs from the analysis of the CONUS RUN-1 data are shown in the lower plot of Figure 3, where they are compared with similar bounds deduced from CsI(Na) data of the COHERENT experiment.⁵ For illustrative purposes, the parameter points of the example BSM signal rates, shown in the upper plot of Figure 3, are marked with crosses. Although CONUS has not observed a CE ν NS signal yet, we place competitive bounds on the tensor NSI couplings ϵ_{ee}^{uT} and ϵ_{ee}^{dT} .⁶ This is due to the signal's

⁵For the extraction of limits shown throughout this paper, we used the tool WebPlotDigitizer [135].

⁶Note that the indices here, referring to the electron (anti)neutrinos involved in the new scattering process, are not to be confused with the indices of eV_{ee} , referring to the ionization energy.

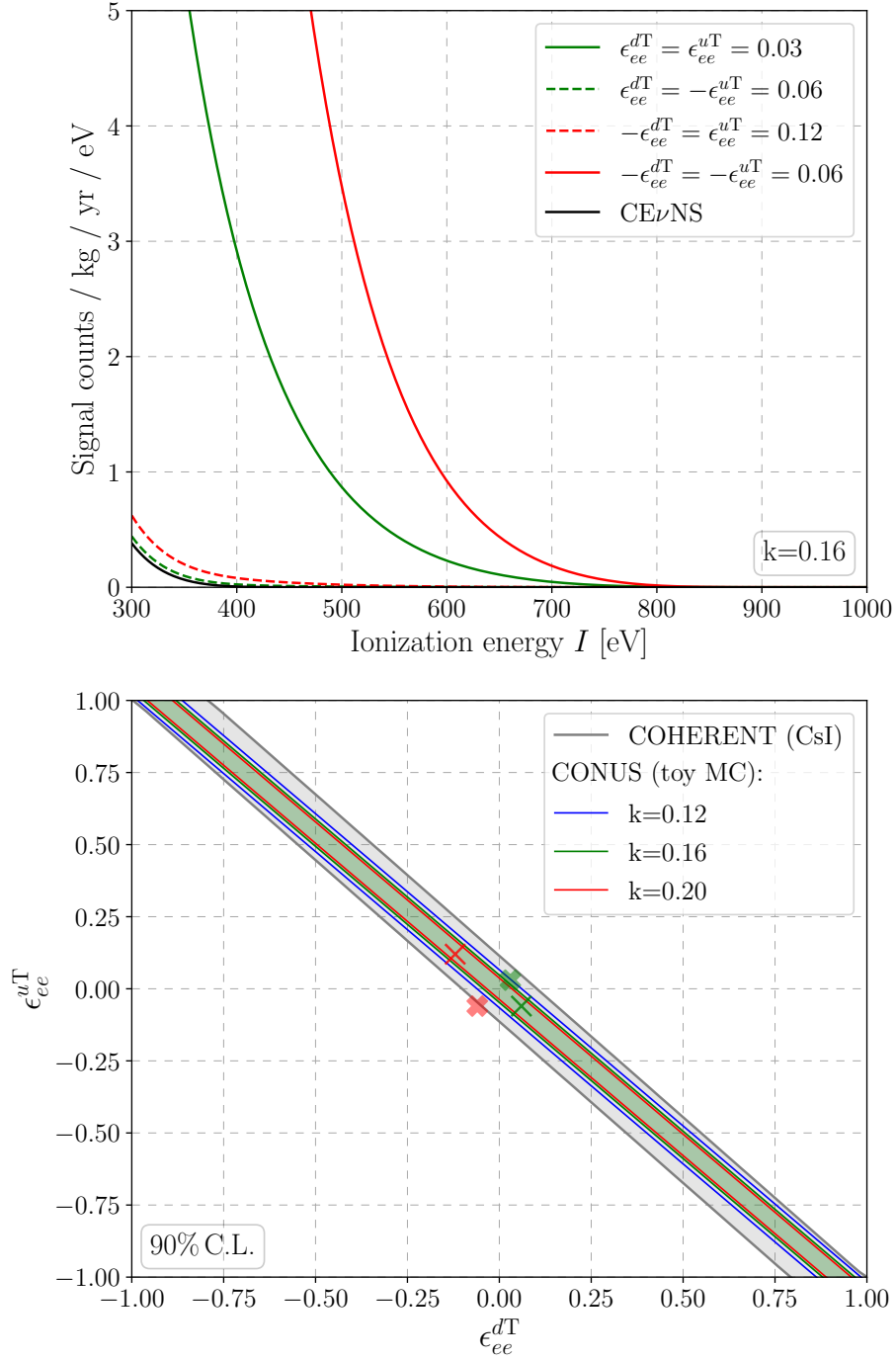


Figure 3. Top: Expected tensor NSI signals of detector C1 for a quenching parameter of $k = 0.16$ and different coupling values from all quadrants in comparison to the standard $\text{CE}\nu\text{NS}$ signal. Due to a different chiral structure, additional tensor NSIs can only enhance the expected signal. Bottom: Allowed regions (at 90% C.L.) of tensor NSI couplings ϵ_{ee}^{uT} and ϵ_{ee}^{dT} deduced from the RUN-1 CONUS data set. The exemplary points of the upper plot are marked with crosses, where bold crosses indicate couplings that are (almost) excluded, i.e. the solid lines from above. Normal crosses refer to coupling combinations that cannot be excluded with the current data set, i.e. the dashed lines. In addition, constraints (90% C.L.) obtained from COHERENT data are plotted for comparison, cf. Ref. [7].

higher extent (compared to SM CE ν NS) and the low background levels obtained below 1 keV $_{ee}$. Here, the quenching factor's impact is of minor importance since, for the values considered, the tensor NSI signal lies way above the CONUS energy threshold allowing for bounds that are mainly dominated by the experimental conditions like background and exposure. Figure 3 furthermore illustrates how the degeneracy between the two NSI couplings, ϵ_{ee}^{uT} and ϵ_{ee}^{dT} , can be broken. The different slopes of the limit bands that are visible for CONUS and COHERENT are due to the different detector isotopes used in the experiments. In general, they allow for breaking the degeneracy of the couplings. However, with data obtained so far the difference between the detector materials CsI and Ge (in terms of N and Z) is not sufficient to have a substantial impact on the combined allowed regions.

Since NSIs are by definition induced by a new heavy mediator that has been integrated out, we can translate the bounds we found for the tensor NSIs into a scale at which this effective description is expected to break down. This scale, where new physics gets probed, is given by $\Lambda \approx g_x/g \cdot M_W/\sqrt{\epsilon} \sim M_W/\sqrt{\epsilon}$, cf. Ref. [35], and, in the case of our determined limits, turns out to be higher than ~ 360 GeV. Hence, with increasing sensitivity low energy experiments like CONUS might probe physics at energy scales comparable to the LHC (TeV scale).

3.1.2 Vector-type interaction

Using the same notation as for the tensor-type NSIs, the vector-type NSIs represent a four-fermion interaction described by the operator

$$\mathcal{O}_{\text{NSI}}^{qV} = (\bar{\nu}_\alpha \gamma^\mu L \nu_\beta) (\bar{q} \gamma_\mu P q) + \text{h.c.}, \quad (3.4)$$

with left- and right-handed projection operators $P = \{L, R\}$. Since this new vector-type interaction exhibits a structure similar to the conventional SM CE ν NS, the related couplings to quarks can be directly absorbed in the weak charge, cf. Eq. (2.1): $\mathcal{Q}_W \rightarrow \mathcal{Q}_{\text{NSI}}^V$. Furthermore, the operator in Eq. (3.4) can trigger a flavor change among the involved neutrinos and, thus, neutrino-nucleus scattering might become flavor-dependent. In its most general version, the modified weak charge now reads, cf. Ref. [32],

$$\begin{aligned} \mathcal{Q}_{\text{NSI}}^V = & \left(g_V^p + 2\epsilon_{\alpha\alpha}^{uV} + \epsilon_{\alpha\alpha}^{dV} \right) Z + \left(g_V^n + \epsilon_{\alpha\alpha}^{uV} + 2\epsilon_{\alpha\alpha}^{dV} \right) N \\ & + \sum_{\alpha,\beta} \left[\left(2\epsilon_{\alpha\beta}^{uV} + \epsilon_{\alpha\beta}^{dV} \right) Z + \left(\epsilon_{\alpha\beta}^{uV} + 2\epsilon_{\alpha\beta}^{dV} \right) N \right], \end{aligned} \quad (3.5)$$

where the first line represents the flavor-preserving interactions (including SM CE ν NS) and the second line the flavor-changing interactions. As for tensor NSIs, with reactor antineutrinos it is only possible to probe effective couplings of electron-type, i.e. ϵ_{ee}^{uV} and ϵ_{ee}^{dV} . In contrast, with π -DAR beams it is possible to investigate several types of couplings since they contain muon (anti)neutrinos as well. Investigations of the COHERENT data have already led to bounds on such couplings, either assuming one to be non-vanishing at a time, e.g. Ref. [9, 10], or in a combined approach with oscillation data that takes into account flavor-changing couplings as well, cf. Ref. [139].

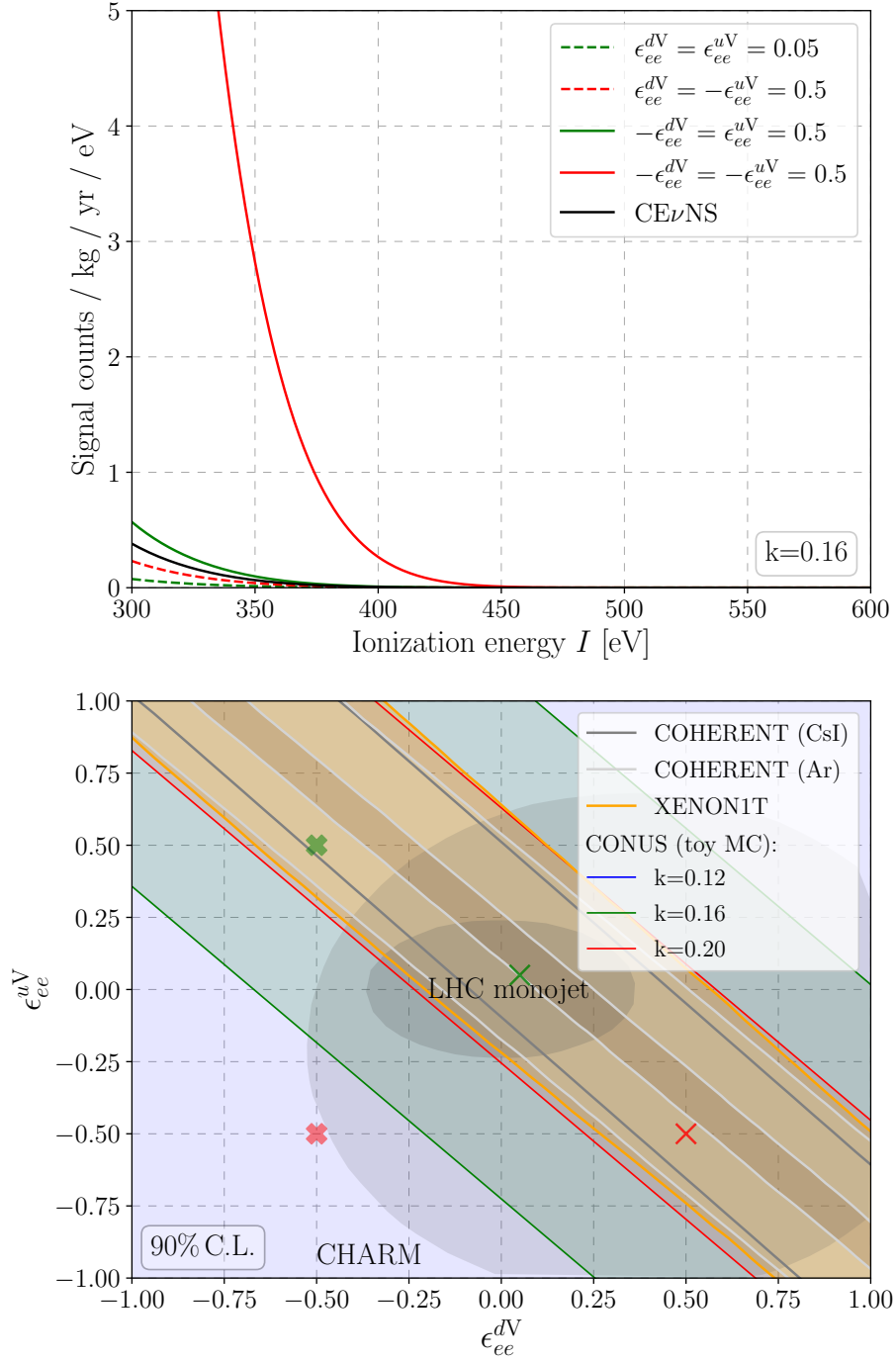


Figure 4. Top: Expected vector NSI signals in detector C1, assuming a quenching parameter of $k = 0.16$ and different coupling values from all quadrants in comparison to the standard CE ν NS signal. Note that, depending on the explicit couplings, destructive interference between the vector NSIs and the SM signals is possible and the expected number of events can be reduced (with respect to the pure SM case). Bottom: Allowed regions (at 90% C.L.) of vector NSI couplings ϵ_{ee}^{uV} and ϵ_{ee}^{dV} deduced from the RUN-1 CONUS data set. As in Figure 3, the example points of the upper plot are marked with crosses, where bold crosses indicate signals stronger than the SM expectation and normal crosses point to the parameter space of destructive interference between the SM and BSM channels. For comparison, constraints (90% C.L.) obtained from COHERENT (CsI [10] and Ar [5]) data and the Xenon1T experiment [136] are shown. Further existing limits, e.g. from CHARM (90% C.L.) [137] and LHC monojet searches (95% C.L.) [138] are indicated with grey elliptic regions.

The expectation of potential vector NSI signals within detector C1 are shown in the upper plot of Figure 4 together with the corresponding SM $\text{CE}\nu\text{NS}$ signal. Both signals share the same kinematic cut-off and due to the same chiral structure, destructive interference is possible in some regions of the parameter space. Thus, $(\text{CE}\nu\text{NS} + \text{vector NSI})$ signal rates smaller than the expected $\text{CE}\nu\text{NS}$ rate alone are possible in the context of vector NSIs as indicated by the dashed lines in the upper plot of Figure 4.

In contrast to tensor NSIs, the vector NSI case does not benefit from an extent to higher energies. As a consequence, we cannot hope to obtain equally strong bounds as COHERENT. This effect is visible in the lower plot of Figure 4, which shows the deduced limits on vector NSIs from the CONUS RUN-1 data set in comparison to the existing limits, i.e. from the experiments COHERENT and Xenon1T. It is apparent that the strength of the limits for vector NSIs strongly depends on the quenching factor, which is due to the fact that the quenching factor significantly influences the expected number of events in the ROI. Comparing the derived CONUS limits on vector NSIs for the currently favored quenching value of $k = 0.16$ to bounds from other experiments, we find that they are currently subdominant. Furthermore, resolving the region of destructive interference is beyond the current experimental reach. However, further experimental improvements that could lead to a future detection of $\text{CE}\nu\text{NS}$ would also significantly improve the sensitivity to vector NSIs and could even allow to probe the parameter region of strong destructive interference.

3.2 Simplified mediator models

Another class of models that can be constrained with CONUS data are so-called ‘simplified models’ that have been intensively studied, e.g. in the dark matter searches at the LHC [140–142]. Although such kind of models have to be taken with care [143–145], they experience great popularity since they do not need to be fully specified at high energy. Besides dark matter and neutrino physics, this simple framework is applied in various contexts, such as in searches for two Higgs doublet models at the LHC [146] or for leptoquark investigations of B-mesons anomalies [147]. For neutrino-electron scattering or neutrino-nucleus scattering measurements, such models are interesting since the mediators can have an impact on the recorded recoil spectra, most pronounced for mediator masses that are smaller than the maximal momentum transfer. Thus, experiments using reactor antineutrinos can, especially in the mediator mass region below ~ 10 MeV, be even more sensitive than experiments using π -DAR sources. In the following, we investigate signatures of new scalar and vector mediators that might scatter off nuclei or electrons by using the CONUS RUN-1 data sets as defined in Table 2.

3.2.1 Light vector bosons

New Z -like vector bosons arise in simple $U(1)$ extensions of the SM and have been studied in various scenarios such as gauged $B-L$, sequential SM and multiple others, cf. e.g. Refs. [148, 149]. Setting the model-building aside, we can work with an effective Lagrangian including

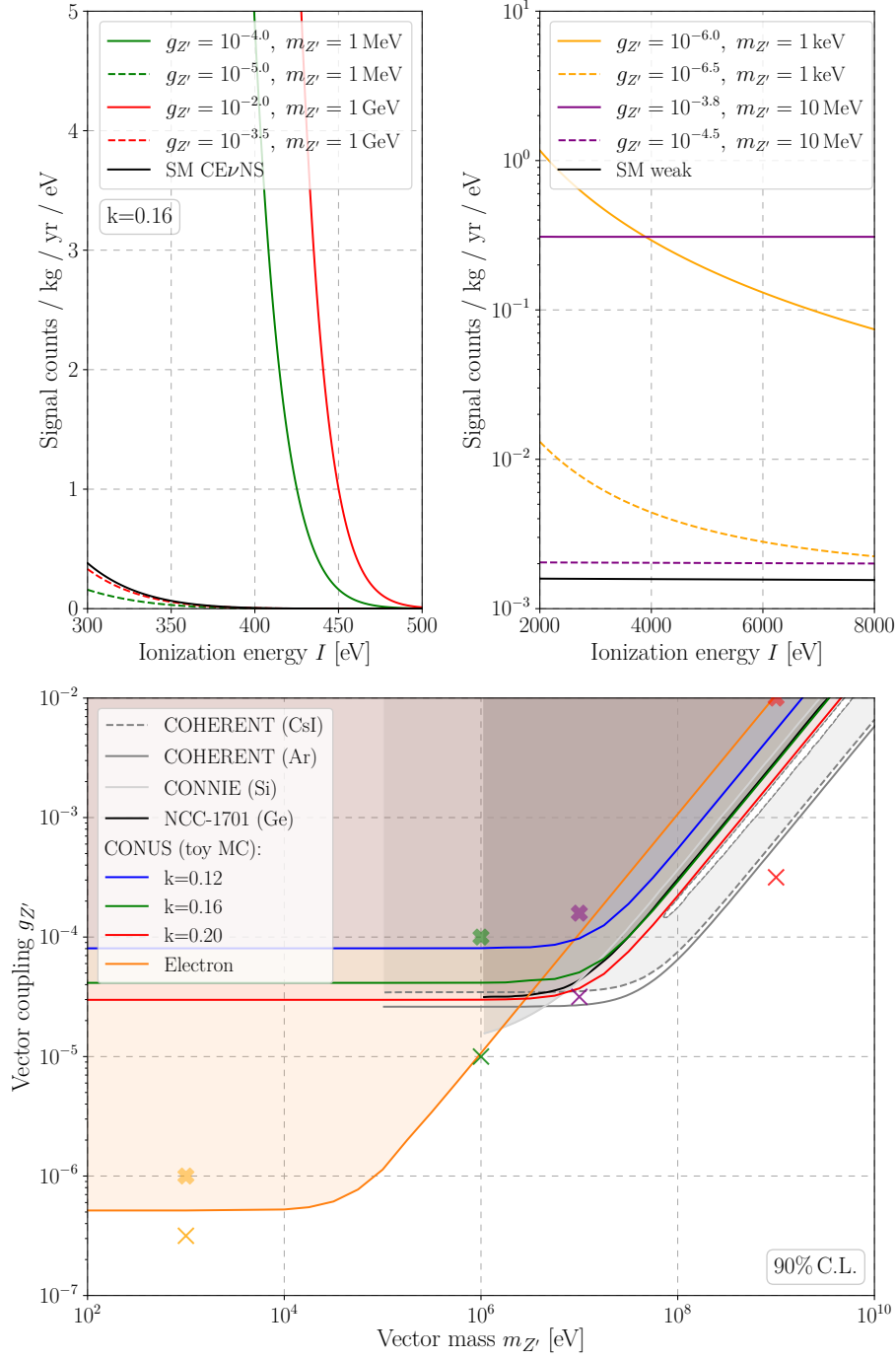


Figure 5. Top: Expected light vector signals of detector C1 in the low energy region below 500 eV_{ee} for a quenching parameter of $k = 0.16$ (left) and in the higher energy region between 2 and 8 keV_{ee} (right) for different couplings and masses in comparison to the SM signals of CE ν NS and elastic neutrino-electron scattering, respectively. Bottom: Limits (90% C.L.) on the light vector mediator parameters ($m_{Z'}, g_{Z'}$) deduced from CE ν NS and neutrino-electron scattering with the RUN-1 CONUS data sets. The exemplary parameter points of the upper signal spectra are shown as well. Bold crosses indicate parameter points that can already be excluded while regular crosses refer to points that are still allowed. For comparison, limits obtained from COHERENT (CsI and Ar) data (90% C.L.) [54], CONNIE (95% C.L.) [53] as well as NCC-1701 (95% C.L., quenching according to Ref. [96]) [71] are shown. The ‘island of non-exclusion’ in the COHERENT limits is due to destructive interference and does not appear in the CONNIE, CONUS and NCC-1701 limits as these experiments have not yet reached the necessary sensitivity.

vector-type interactions of neutrinos, quarks and electrons, of the form

$$\mathcal{L}_{Z'} = Z'_\mu \left(g_{Z'}^{\nu V} \bar{\nu}_L \gamma^\mu \nu_L + g_{Z'}^{e V} \bar{e} \gamma^\mu e + g_{Z'}^{q V} \bar{q} \gamma^\mu q \right) + \frac{1}{2} m_{Z'}^2 Z'_\mu Z'^\mu, \quad (3.6)$$

with vector-type couplings $g_{Z'}^{xV}$ ($x = \{\nu, e, q\}$ and $q = \{u, d\}$) and mass of the new vector boson $m_{Z'}$. Within this simplified model, we only include interactions of SM neutrinos, i.e. left-handed neutrinos and right-handed antineutrinos, and do not take into account characteristic features like kinetic or mass mixing. In the following, we investigate two reaction channels that arise from Eq. (3.6): neutrino-nucleus as well as neutrino-electron scattering. In both cases, the light vector boson adds a new reaction channel that can interfere with the SM one, since both share the same final state. For our investigation, we assume universal couplings, i.e. $g_{Z'} \equiv g_{Z'}^{\nu V} = g_{Z'}^{e V} = g_{Z'}^{u V} = g_{Z'}^{d V}$, allowing us to reduce the parameter space to only two parameters: $(m_{Z'}, g_{Z'})$.

The cross section of neutrino-nucleus scattering including a light vector contribution can be expressed as [7]

$$\left(\frac{d\sigma}{dT_A} \right)_{\text{CE}\nu\text{NS}+Z'} = \mathcal{G}_{Z'}^2(T_A) \left(\frac{d\sigma}{dT_A} \right)_{\text{CE}\nu\text{NS}}, \quad (3.7)$$

with the SM cross section as given in Eq. (2.1) and the prefactor $\mathcal{G}_{Z'}$ defined as⁷

$$\mathcal{G}_{Z'}(T_A) = 1 + \frac{g_{Z'}^{\nu V}}{\sqrt{2}G_F} \frac{\mathcal{Q}_{Z'}}{\mathcal{Q}_W} \frac{1}{2m_A T_A + m_{Z'}^2}. \quad (3.8)$$

The nuclear charge associated to the light vector mediator is given by [20]

$$\mathcal{Q}_{Z'} = \left(2g_{Z'}^{uV} + g_{Z'}^{dV} \right) Z + \left(g_{Z'}^{uV} + 2g_{Z'}^{dV} \right) N \rightarrow 3g_{Z'}(Z + N), \quad (3.9)$$

where the last step is due to our assumption of universal couplings to leptons and quarks. As a result, the light vector part of Eq. (3.8) scales as $g_{Z'}^2$, leading to a proportionality of up to $g_{Z'}^4$ in the cross section of Eq. (3.7). A second effect that becomes visible in Eq. (3.8) is the possibility of destructive interference, originating from a negative coupling, which leads to ‘islands of non-exclusion’ in the exclusion plot, cf. COHERENT limits in Figure 5. In this case the prefactor $\mathcal{G}_{Z'}$ turns from the SM value 1 into -1 due to the Z' contribution, leaving the resulting cross section invariant, cf. Eq. (3.7). However, reactor experiments do not have the sensitivity to observe this effect yet, cf. Figure 5.

It is worth to mention that there is in principle a connection between the vector mediators discussed here and the previously discussed vector NSIs. Integrating out the vector mediator allows for a mapping between the Z' couplings and mass and the ϵ -parameters of vector NSIs [150]

$$\epsilon_{\alpha\beta}^{qV} = \frac{\left(g_{Z'}^{\nu V} \right)_{\alpha\beta} g_{Z'}^{qV}}{2\sqrt{2}G_F M_{Z'}^2}, \quad (3.10)$$

⁷In literature, other definitions of $\mathcal{G}_{Z'}$ can be found which differ by a factor of $\frac{1}{2}$. As mentioned before, these differences are due to different definitions of \mathcal{Q}_W .

where the couplings $(g_{Z'}^{\nu V})_{\alpha\beta}$ can in general be flavor-dependent. However, integrating out the mediating particle is only possible when the mediator is significantly heavier than the momentum transfer in the scattering process. Since this condition is violated for light mediators, we discuss the two models separately.

In addition to neutrino-nucleus scattering, we also look at the influence of a new vector mediator on neutrino-electron scattering. The corresponding cross section is given by [19]

$$\left(\frac{d\sigma}{dT_e}\right)_{\nu e+Z'} = \left(\frac{d\sigma}{dT_e}\right)_{\nu e} + \frac{\sqrt{2}G_F m_e g_V g_{Z'}^{\nu V} g_{Z'}^{eV}}{\pi(2m_e T_e + m_{Z'}^2)} + \frac{m_e (g_{Z'}^{\nu V} g_{Z'}^{eV})^2}{2\pi(2m_e T_e + m_{Z'}^2)^2}, \quad (3.11)$$

with the electron vector coupling to Z bosons $g_V = -\frac{1}{2} + 2\sin^2\theta_W$. By comparing the last term of Eq. (3.11) to Eq. (3.7), we can see how neutrino-electron scattering can enable us to set stronger limits for small Z' masses. For $m_{Z'}^2 \ll 2m_e T_e$, the electron mass m_e in the numerator cancels out and we end up with $4m_e T_e^2$ in the denominator. Comparing this to the denominator $4m_A T_A^2$ in Eq. (3.7) (together with Eq. (2.1)), we note that the smaller electron mass enhances our cross section and thus leads to a stronger limit for universal couplings in this region of our parameter space.

Exemplary event spectra for neutrino-nucleus and neutrino-electron scattering for detector C1 are shown in the upper plots of Figure 5 for two different masses of the Z' and two different couplings for each mass. The conventional SM channels are illustrated for comparison. Especially, note the change in shape for elastic neutrino-electron scatterings of the shown parameter points in the upper right plot of Figure 5 which illustrates the different behavior for the denominator in Eq. (3.11) mentioned above. In the lower plot of Figure 5, the resulting limits of our analysis are depicted in the $(m_{Z'}, g_{Z'})$ -plane together with bounds from COHERENT [7, 52, 54, 55], CONNIE [53] and NCC-1701 [71]. For Z' masses above 10 MeV, the strongest bounds can be set by π DAR experiments because of their higher neutrino energies, while for smaller masses reactor experiments can set competitive or stronger bounds. Furthermore, the limits we can set from neutrino-electron scattering are stronger than the ones from neutrino-nucleus scattering for $m_{Z'} \lesssim 10$ MeV as explained before. With the current data set and the most favored quenching value $k = 0.16$, the lowest coupling value that can be probed with CE ν NS is $\sim 4 \cdot 10^{-5}$. In the case of elastic neutrino-electron scattering the coupling can be constrained down to $\sim 6 \cdot 10^{-7}$ for lowest mediator masses.

Besides the bounds from CE ν NS experiments shown in Figure 5, there exists a plethora of bounds on vector mediators from various other types of experiments, especially in the context of a gauged $U(1)_{B-L}$ symmetry. This includes searches for dielectron resonances at ATLAS [151], beam dump investigations [152, 153], bounds from neutrino-electron scattering [154, 155] as well as dark photon searches at BaBar [156, 157] and LHCb [158]. Numerous collections of bounds can be found e.g. in Refs. [148, 159] for general models and Ref. [160] for $B-L$ extensions. While focusing on the strengths of the limits derived in this work in context of CE ν NS experiments, we mention the broader scope of bounds for the interested reader.

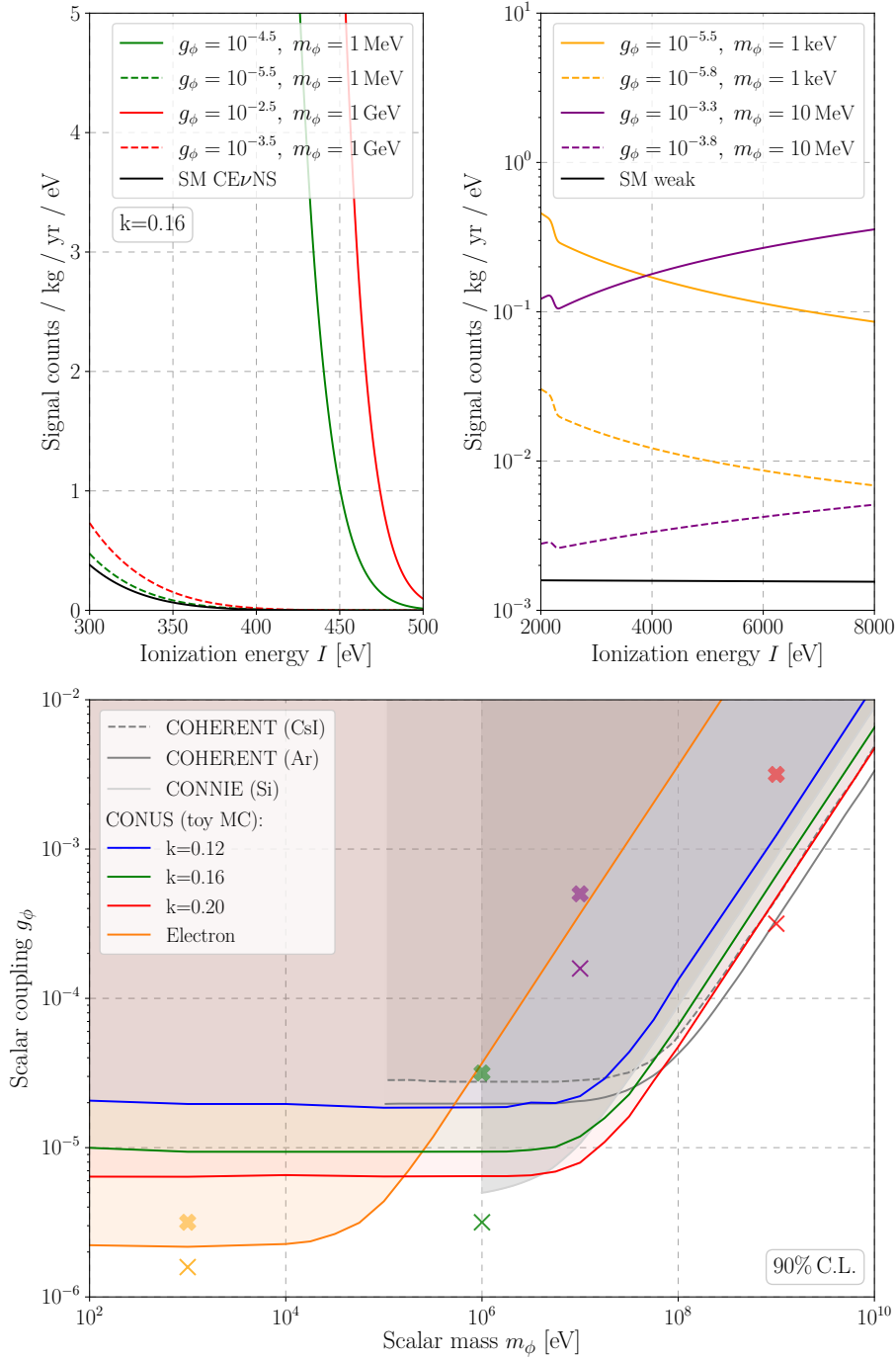


Figure 6. Top: Expected light scalar signals of detector C1 in the low energy region below 500 eV_{ee} for a quenching parameter of $k = 0.16$ (left) and in the higher energy region between 2 and 8 keV_{ee} (right) for different couplings and masses in comparison to the SM signals of CE ν NS and elastic neutrino-electron scattering, respectively. Note that the wiggles at $\sim 2 \text{ keV}$ are not artifacts but result from the applied reactor model. Bottom: Limits (90% C.L.) on the light scalar mediator parameters (m_ϕ, g_ϕ) deduced from CE ν NS and neutrino-electron scattering with the RUN-1 CONUS data sets. As before, we point out the exemplary parameter points of the signal spectra above. Bold crosses indicate parameter points that can already be excluded while regular crosses refer to points that are still in agreement with the data. For comparison, limits obtained from COHERENT (CsI and Ar) data (90% C.L.) [161] and CONNIE (95% C.L.) [53] are shown.

3.2.2 Light scalar bosons

Finally, we investigate elastic neutrino-nucleus and neutrino-electron scattering induced by a light scalar mediator ϕ . We select a simple benchmark model, i.e. a CP-even massive real scalar boson with pure scalar-type couplings to the first generation of leptons and quark. The Lagrangian of this simplified model is given by [19]

$$\mathcal{L}_\phi = \phi \left(g_\phi^{qS} \bar{q}q + g_\phi^{eS} \bar{e}e + g_\phi^{\nu S} \bar{\nu}_R \nu_L + \text{h.c.} \right) - \frac{1}{2} m_\phi^2 \phi^2, \quad (3.12)$$

with the individual scalar coupling g_ϕ^{xS} ($x = \{\nu, e, q\}$ and $q = \{u, d\}$). As for the vector mediator case, we put model-building aspects aside and work with this simplified model even though a realistic low-energy model needs to be more complex to become consistent with the SM symmetries [162]. Along the line of Refs. [7, 8], we also ignore resulting consequences for neutrino phenomenology in this analysis.

The associated neutrino-nucleus scattering cross section takes the form [7, 19]

$$\left(\frac{d\sigma}{dT_A} \right)_{\text{CE}\nu\text{NS}+\phi} = \left(\frac{d\sigma}{dT_A} \right)_{\text{CE}\nu\text{NS}} + \frac{(g_\phi^{\nu S} \mathcal{Q}_\phi)^2 m_A^2 T_A}{4\pi E_\nu^2 (2m_A T_A + m_\phi^2)^2}, \quad (3.13)$$

with the nuclear charge associated to the light scalar mediator being [163]

$$\mathcal{Q}_\phi = \sum_{N,q} g_\phi^{qS} \frac{m_N}{m_q} f_{T,q}^{(N)} \rightarrow g_\phi (14N + 15.1Z). \quad (3.14)$$

The last step is obtained by assuming a universal coupling to leptons and quarks, and summing up all nucleon form factors $f_{T,q}^{(N)}$, which incorporate the effective low-energy couplings of the scalar ϕ to the nucleons $N = \{p, n\}$, cf. Ref. [163]. Thus, with the assumption of a universal coupling, the corresponding part of the cross section in Eq. (3.13) scales with g_ϕ^4 and the model's parameter space is now spanned by only two parameters, the scalar mass m_ϕ and its couplings to fermions g_ϕ . Since the scalar-neutrino interaction flips chirality (in contrast to the chirality-conserving SM case), there is no interference and the scalar cross section is simply added to the SM CE ν NS signal. Another interesting aspect that appears in Eq. (3.13) is the scaling with the recoil energy T_A in comparison to the vector case, cf. Eq. (3.7). For the scalar mediator, the corresponding part of the cross section scales with $1/T_A$, whereas in the vector case it scales with $1/T_A^2$, leading to a less steep signal.

The Lagrangian in Eq. (3.12) also induces an additional interaction between neutrinos and electrons. Thus, there is a contribution to the cross section for neutrino-electron scattering, leading in total to [19]

$$\left(\frac{d\sigma}{dT_e} \right)_{\nu e+\phi} = \left(\frac{d\sigma}{dT_e} \right)_{\nu e} + \frac{(g_\phi^{\nu S} g_\phi^{eS})^2 m_e^2 T_e}{4\pi E_\nu^2 (2m_e T_e + m_\phi^2)^2}. \quad (3.15)$$

Under the assumption of universal scalar couplings, this shrinks down to the same quartic dependence as for neutrino-nucleus scattering, i.e. $(g_\phi^{\nu S} g_\phi^{eS})^2 \rightarrow g_\phi^4$. As for the case of a light vector mediator, the denominator in Eq. (3.15) can be separated into two different

cases, i.e. $2m_e T_e \ll m_\phi^2$ and $2m_e T_e \gg m_\phi^2$, which correspond to the different behaviors of the obtained limit curves.

The expected event rates and the signal shape of elastic neutrino-nucleus and neutrino-electron scattering mediated by a light scalar are depicted in the upper left and right plots of Figure 6, respectively. For comparison to the different signal expectations (two coupling values for each of the two scalar mediator masses), we also indicated the SM signal channels. By comparing the upper left plots of Figure 5 and Figure 6, one notes the previously mentioned difference in steepness or scaling with T_A between the scalar and the vector mediator. Further, this different scaling yields a different behavior for electron scatterings at higher energies, cf. upper right plots of Figure 5 and Figure 6. Here, the electron scattering exhibits a linear dependence on the recoil energy. In the end, this difference leads to stronger limits for the scalar mediator, which are displayed in the lower plot of Figure 6. For comparison, we also show the limits obtained from COHERENT and CONNIE and marked the parameter points of the upper plots with crosses. Again, we highlighted both cases, points that are already excluded as well as points that still agree with the used data set. The lowest coupling value that can be probed with CE ν NS is $\sim 10^{-5}$ for the currently most favoured quenching value of $k = 0.16$, while elastic neutrino-electron scattering allows us to constrain the coupling down to $\sim 2 \cdot 10^{-6}$ for lowest mediator masses. As before, competitive CE ν NS bounds can be gained for especially low mediator masses, i.e. below ~ 1 MeV, which is attributed to the low neutrino energy provided by the reactor antineutrinos.

4 Conclusions

The CONUS experiment aims at the detection of CE ν NS with four HPGe detectors in a sophisticated shield at 17.1 m-distance to the 3.9 GW_{th} core of the nuclear power plant in Brokdorf, Germany. After a first spectral analysis devoted to the CE ν NS search in CONUS data, cf. Ref. [6], we used here RUN-1 data to constrain several BSM models. In particular, we searched for modifications of CE ν NS due to NSIs of both tensor and vector type as well as light vector and scalar mediators. The latter two have been tested as so-called simplified models on their impact on CE ν NS and neutrino-electron scattering. We make use of a similar analysis procedure that has already been used in the first CE ν NS investigation, including all systematic uncertainties therein. Small modifications have been applied due to the inclusion of uncertainties in the background MC simulation used in the higher energy spectrum, cf. Section 2 and the background-related publication [93]. Further, a refined noise edge parameterization was applied, leading to energy thresholds of the ROIs that are slightly lower compared to the analysis in Ref. [6].

During our analysis, the likelihood function, cf. Eq. (2.7), was varied with the cross sections of the individual models. Limits were derived from data of three detectors in the experiment's first data collection period RUN-1. For the investigation of neutrino-electron scatterings above 2 keV_{ee}, a data set with extended exposure is used to increase the experimental sensitivity, cf. Table 2 for an overview of all data sets used throughout this work. For CONUS, quenching, i.e. the fraction of nuclear recoil energy available as

ionization for signal formation, is the least known input parameter and thus the dominating uncertainty. In combination with neutrino energies below 10 MeV, this renders $\text{CE}\nu\text{NS}$ measurements at a reactor site especially demanding. Thus, we derive our BSM constraints for three different quenching parameters which span the range of currently favored values: $k = \{0.12, 0.16, 0.20\}$, where k represents the quenching factor at recoil energies around 1 keV $_{ee}$, cf. Section 2. The obtained bounds, except in the case of vector NSIs, are at least in some regions of the parameter space competitive with existing bounds from other $\text{CE}\nu\text{NS}$ experiments, cf. Section 3. For tensor NSIs, we present limits that represent the world’s best limits on electron-type couplings to up- and down-type quarks from $\text{CE}\nu\text{NS}$. The scale of associated BSM physics can be constrained to lie above ~ 360 GeV, cf. Figure 3. Corresponding bounds in the case of vector-type NSIs are highly dependent on the quenching parameter k and at the moment not competitive to existing bounds due to the limited sensitivity of CONUS on the $\text{CE}\nu\text{NS}$ signal itself, cf. Figure 4. Since reactor antineutrinos are emitted at lower energies than neutrinos from a π -DAR source, our bounds on light scalar or vector mediators are stronger at smaller mediator masses. For higher masses, neutrinos from a π -DAR source yield currently the strongest $\text{CE}\nu\text{NS}$ limits, cf. Figure 5 and Figure 6. Moreover, limits obtained from electron scatterings are stronger than the ones obtained from $\text{CE}\nu\text{NS}$ for masses below ~ 10 MeV and ~ 1 MeV for vector and scalar mediators, respectively. However, we note that the shown parameter space region can only be excluded for models that incorporate electron and quark interactions with universal couplings. For more specific frameworks, i.e. nucleophilic/leptophilic mediators or non-universal couplings, the obtained contours have to be viewed individually and/or with appropriate corrections.

After a series of experimental improvements, i.e. an advanced data acquisition system and more stable environmental conditions, CONUS continues data collection. Thus, for the future we expect our bounds to strengthen with more exposure. After the reactor shutdown at the end of 2021, additional OFF data are expected to increase the experimental sensitivity. Further, the CONUS Collaboration developed a program to pin down the dominating uncertainty related to the not well known quenching factor in germanium. Our recently conducted measurement is indicating a quenching factor value that agrees with the currently favored one and that follows the Lindhard theory down to nuclear recoils of a few keV, cf. Ref. [164]. With a future $\text{CE}\nu\text{NS}$ detection via the CONUS set-up, we expect stronger bounds, especially in the case of vector NSIs. Then, investigation of further BSM topics like neutrino electromagnetic properties, sterile neutrino and dark matter will lead to further constraints. An investigation of neutrino magnetic moments via neutrino–electron scattering at energies above 2 keV $_{ee}$ can be found in Ref. [114].

While first BSM constraints of COHERENT, CONNIE, CONUS and NCC-1701 at DRESDEN-II [71] already revealed the huge potential of $\text{CE}\nu\text{NS}$ measurements, which can be viewed as a proof of principle by itself, more experiments are going to contribute further knowledge by using different target elements and detection technologies. There are various endeavors close to nuclear reactors and first sensitivity studies for the European Spallation Source (ESS) already exist, cf. Refs. [165, 166]. Taking advantage of these different neutrino sources, in terms of complementary measurements between reactor and neutrino beam experiments, allows for further interesting physics investigations [167, 168].

Therefore, the next generation of CE ν NS experiments promises an active field with new approaches and interesting possibilities [31, 169–173] and represents another step towards the era of precision neutrino physics.

Acknowledgments

We thank the technical and administrative staff who helped building the experiment, in particular the MPIK workshops and Mirion Technologies (Canberra) in Lingolsheim. We express our gratitude to the PreussenElektra GmbH for enduring and prolific support and for hosting the CONUS experiment. Moreover, we thank Dr. S. Schoppmann (MPIK) for assistance on the analysis and Dr. M. Seidl (PreussenElektra GmbH) for providing simulation data on the fission rate evolution over a reactor cycle. Further thanks are directed to K. Zink and the MPIK IT department for their support concerning the institute’s cluster infrastructure. We are grateful to G. Vogt (MPIK) for providing an artist’s view of our experiment (Figure 1). The CONUS experiment is supported financially by the Max Planck Society (MPG) and T. Rink by the IMPRS-PTFS as well as by the German Research Foundation (DFG) through the research training group GRK 1940.

References

- [1] D. Z. Freedman, *Coherent effects of a weak neutral current*, *Physical Review D* **9** (1974) 1389.
- [2] D. L. Tubbs and D. N. Schramm, *Neutrino Opacities at High Temperatures and Densities*, *The Astrophysical Journal* **201** (1975) 467.
- [3] A. Drukier and L. Stodolsky, *Principles and Applications of a Neutral Current Detector for Neutrino Physics and Astronomy*, *Phys.Rev.D* **30** (1984) 2295.
- [4] COHERENT collaboration, D. Akimov et al., *Observation of Coherent Elastic Neutrino-Nucleus Scattering*, *Science* **357** (2017) 1123 [1708.01294].
- [5] COHERENT collaboration, D. Akimov et al., *First Measurement of Coherent Elastic Neutrino-Nucleus Scattering on Argon*, *Phys. Rev. Lett.* **126** (2021) 012002 [2003.10630].
- [6] CONUS collaboration, H. Bonet et al., *Constraints on Elastic Neutrino Nucleus Scattering in the Fully Coherent Regime from the CONUS Experiment*, *Phys. Rev. Lett.* **126** (2021) 041804 [2011.00210].
- [7] D. K. Papoulias and T. S. Kosmas, *COHERENT constraints to conventional and exotic neutrino physics*, *Phys.Rev.D* **97** (2018) [1711.09773].
- [8] J. Billard, J. Johnston and B. J. Kavanagh, *Prospects for exploring New Physics in Coherent Elastic Neutrino-Nucleus Scattering*, *JCAP* **11** (2018) 016 [1805.01798].
- [9] A. N. Khan and W. Rodejohann, *New physics from COHERENT data with an improved quenching factor*, *Phys.Rev.D* **100** (2019) [1907.12444].
- [10] D. K. Papoulias, *COHERENT constraints after the COHERENT-2020 quenching factor measurement*, *Phys.Rev.D* **102** (2020) [1907.11644].
- [11] D. Z. Freedman, D. N. Schramm and D. L. Tubbs, *The Weak Neutral Current and its Effects in Stellar Collapse*, *Annual Review of Nuclear Science* **27** (1977) 167.

- [12] P. S. Amanik and G. M. Fuller, *Stellar Collapse Dynamics With Neutrino Flavor Changing Neutral Currents*, *Phys.Rev.D* **75** (2007) [[astro-ph/0606607](#)].
- [13] K. G. Balasi, K. Langanke and G. Martínez-Pinedo, *Neutrino–nucleus reactions and their role for supernova dynamics and nucleosynthesis*, *Prog.Part.Nucl.Phys.* **85** (2015) 33 [[1503.08095](#)].
- [14] M. Biassoni and C. Martinez, *Study of supernova ν -nucleus coherent scattering interactions*, *Astropart.Phys.* **36** (2012) 151 [[1110.3536](#)].
- [15] V. Brdar, M. Lindner and X.-J. Xu, *Neutrino astronomy with supernova neutrinos*, *JCAP* **04** (2018) 025 [[1802.02577](#)].
- [16] DARKSIDE 20K collaboration, P. Agnes et al., *Sensitivity of future liquid argon dark matter search experiments to core-collapse supernova neutrinos*, *JCAP* **03** (2021) 043 [[2011.07819](#)].
- [17] J. Monroe and P. Fisher, *Neutrino Backgrounds to Dark Matter Searches*, *Phys.Rev.D* **76** (2007) [[0706.3019](#)].
- [18] A. Gutlein, C. Ciemniak, F. von Feilitzsch, N. Haag, M. Hofmann, C. Isaila et al., *Solar and atmospheric neutrinos: Background sources for the direct dark matter search*, *Astropart.Phys.* **34** (2010) 90 [[1003.5530](#)].
- [19] D. G. Cerdeño, M. Fairbairn, T. Jubb, P. A. N. Machado, A. C. Vincent and C. Boehm, *Physics from solar neutrinos in dark matter direct detection experiments*, *JHEP* **05** (2016) 118 [[1604.01025](#)].
- [20] E. Bertuzzo, F. F. Deppisch, S. Kulkarni, Y. F. Perez Gonzalez and R. Zukanovich Funchal, *Dark Matter and Exotic Neutrino Interactions in Direct Detection Searches*, *JHEP* **04** (2017) 073 [[1701.07443](#)].
- [21] C. Boehm, D. G. Cerdeño, P. a. N. Machado, A. Olivares-Del Campo, E. Perdomo and E. Reid, *How high is the neutrino floor?*, *JCAP* **01** (2019) 043 [[1809.06385](#)].
- [22] J. M. Link and X.-J. Xu, *Searching for BSM neutrino interactions in dark matter detectors*, *JHEP* **08** (2019) 004 [[1903.09891](#)].
- [23] D. Aristizabal Sierra, B. Dutta, S. Liao and L. E. Strigari, *Coherent elastic neutrino-nucleus scattering in multi-ton scale dark matter experiments: Classification of vector and scalar interactions new physics signals*, *JHEP* **12** (2019) 124 [[1910.12437](#)].
- [24] K. Patton, J. Engel, G. C. McLaughlin and N. Schunck, *Neutrino-nucleus coherent scattering as a probe of neutron density distributions*, *Phys.Rev.C* **86** (2012) [[1207.0693](#)].
- [25] M. Cadeddu, C. Giunti, Y. F. Li and Y. Y. Zhang, *Average CsI neutron density distribution from COHERENT data*, *Phys. Rev. Lett.* **120** (2018) 072501 [[1710.02730](#)].
- [26] P. Coloma, I. Esteban, M. C. Gonzalez-Garcia and J. Menendez, *Determining the nuclear neutron distribution from Coherent Elastic neutrino-Nucleus Scattering: Current results and future prospects*, *JHEP* **08** (2020) 030 [[2006.08624](#)].
- [27] N. Van Dessel, V. Pandey, H. Ray and N. Jachowicz, *Nuclear Structure Physics in Coherent Elastic Neutrino-Nucleus Scattering*, [2007.03658](#).
- [28] H.-S. Lee, *$\sin^2\theta_W$ theory and new physics*, *J. Univ. Sci. Tech. China* **46** (2016) 470 [[1511.03783](#)].
- [29] B. C. Cañas, E. A. Garcés, O. G. Miranda and A. Parada, *Future perspectives for a weak*

- mixing angle measurement in coherent elastic neutrino nucleus scattering experiments*, *Phys.Lett.B* **784** (2018) 159 [[1806.01310](#)].
- [30] X.-R. Huang and L.-W. Chen, *Neutron Skin in CsI and Low-Energy Effective Weak Mixing Angle from COHERENT Data*, *Phys. Rev. D* **100** (2019) 071301 [[1902.07625](#)].
- [31] G. Fernandez-Moroni, P. A. N. Machado, I. Martinez-Soler, Y. F. Perez-Gonzalez, D. Rodrigues and S. Rosauero-Alcaraz, *The physics potential of a reactor neutrino experiment with Skipper CCDs: Measuring the weak mixing angle*, *JHEP* **03** (2021) 186 [[2009.10741](#)].
- [32] J. Barranco, O. G. Miranda and T. I. Rashba, *Probing new physics with coherent neutrino scattering off nuclei*, *JHEP* **12** (2005) 021 [[hep-ph/0508299](#)].
- [33] J. Barranco, O. G. Miranda and T. I. Rashba, *Low energy neutrino experiments sensitivity to physics beyond the Standard Model*, *Phys.Rev.D* **76** (2007) [[hep-ph/0702175](#)].
- [34] J. Barranco, A. Bolanos, E. A. Garces, O. G. Miranda and T. I. Rashba, *Tensorial NSI and Unparticle physics in neutrino scattering*, *Int.J.Mod.Phys.A* **27** (2012) [[1108.1220](#)].
- [35] M. Lindner, W. Rodejohann and X.-J. Xu, *Coherent Neutrino-Nucleus Scattering and new Neutrino Interactions*, *JHEP* **03** (2017) 097 [[1612.04150](#)].
- [36] P. Coloma, M. C. Gonzalez-Garcia, M. Maltoni and T. Schwetz, *COHERENT Enlightenment of the Neutrino Dark Side*, *Phys. Rev. D* **96** (2017) 115007 [[1708.02899](#)].
- [37] J. Liao and D. Marfatia, *COHERENT constraints on nonstandard neutrino interactions*, *Phys. Lett. B* **775** (2017) 54 [[1708.04255](#)].
- [38] I. Bischer, W. Rodejohann and X.-J. Xu, *Loop-induced Neutrino Non-Standard Interactions*, *JHEP* **10** (2018) 096 [[1807.08102](#)].
- [39] P. S. Bhupal Dev, K. S. Babu, P. B. Denton, P. A. N. Machado, C. A. Argüelles, J. L. Barrow et al., *Neutrino Non-Standard Interactions: A Status Report*, *SciPost Phys.Proc.* **2** (2019) 001 [[1907.00991](#)].
- [40] C. Giunti, *General COHERENT constraints on neutrino nonstandard interactions*, *Phys. Rev. D* **101** (2020) 035039 [[1909.00466](#)].
- [41] P. B. Denton and J. Gehrlein, *A Statistical Analysis of the COHERENT Data and Applications to New Physics*, *JHEP* **04** (2021) 266 [[2008.06062](#)].
- [42] P. Vogel and J. Engel, *Neutrino Electromagnetic Form-Factors*, *Phys.Rev.D* **39** (1989) 3378.
- [43] C. Giunti and A. Studenikin, *Neutrino electromagnetic interactions: A window to new physics*, *Rev.Mod.Phys.* **87** (2015) 531 [[1403.6344](#)].
- [44] M. Cadeddu, C. Giunti, K. A. Kouzakov, Y. F. Li, A. I. Studenikin and Y. Y. Zhang, *Neutrino Charge Radii from COHERENT Elastic Neutrino-Nucleus Scattering*, *Phys. Rev. D* **98** (2018) 113010 [[1810.05606](#)].
- [45] O. G. Miranda, D. K. Papoulias, M. Tórtola and J. W. F. Valle, *Probing neutrino transition magnetic moments with coherent elastic neutrino-nucleus scattering*, *JHEP* **07** (2019) 103 [[1905.03750](#)].
- [46] M. Cadeddu, F. Dordei, C. Giunti, Y. F. Li, E. Picciau and Y. Y. Zhang, *Physics results from the first COHERENT observation of coherent elastic neutrino-nucleus scattering in argon and their combination with cesium-iodide data*, *Phys. Rev. D* **102** (2020) 015030 [[2005.01645](#)].
- [47] P. deNiverville, M. Pospelov and A. Ritz, *Light new physics in coherent neutrino-nucleus scattering experiments*, *Phys.Rev.D* **92** (2015) [[1505.07805](#)].

- [48] J. B. Dent, B. Dutta, S. Liao, J. L. Newstead, L. E. Strigari and J. W. Walker, *Probing light mediators at ultralow threshold energies with coherent elastic neutrino-nucleus scattering*, *Phys.Rev.D* **96** (2017) [[1612.06350](#)].
- [49] Y. Farzan, M. Lindner, W. Rodejohann and X.-J. Xu, *Probing neutrino coupling to a light scalar with coherent neutrino scattering*, *JHEP* **05** (2018) 066 [[1802.05171](#)].
- [50] J. B. Dent, B. Dutta, D. Kim, S. Liao, R. Mahapatra, K. Sinha et al., *New Directions for Axion Searches via Scattering at Reactor Neutrino Experiments*, *Phys.Rev.Lett.* **124** (2020) [[1912.05733](#)].
- [51] D. Aristizabal Sierra, V. De Romeri, L. J. Flores and D. K. Papoulias, *Axionlike particles searches in reactor experiments*, *JHEP* **03** (2021) 294 [[2010.15712](#)].
- [52] B. Dutta, S. Liao, S. Sinha and L. E. Strigari, *Searching for Beyond the Standard Model Physics with COHERENT Energy and Timing Data*, *Phys.Rev.Lett.* **123** (2019) [[1903.10666](#)].
- [53] CONNIE collaboration, A. Aguilar-Arevalo et al., *Search for light mediators in the low-energy data of the CONNIE reactor neutrino experiment*, *JHEP* **04** (2020) 054 [[1910.04951](#)].
- [54] M. Cadeddu, N. Cargioli, F. Dordei, C. Giunti, Y. F. Li, E. Picciau et al., *Constraints on light vector mediators through coherent elastic neutrino nucleus scattering data from COHERENT*, *JHEP* **01** (2021) 116 [[2008.05022](#)].
- [55] O. G. Miranda, D. K. Papoulias, M. Tórtola and J. W. F. Valle, *Probing new neutral gauge bosons with CE ν NS and neutrino-electron scattering*, *Phys. Rev. D* **101** (2020) 073005 [[2002.01482](#)].
- [56] V. Brdar, W. Rodejohann and X.-J. Xu, *Producing a new Fermion in Coherent Elastic Neutrino-Nucleus Scattering: From Neutrino Mass to Dark Matter*, *JHEP* **12** (2018) 024 [[1810.03626](#)].
- [57] W.-F. Chang and J. Liao, *Constraints on light singlet fermion interactions from coherent elastic neutrino-nucleus scattering*, *Phys. Rev. D* **102** (2020) 075004 [[2002.10275](#)].
- [58] LSND collaboration, A. Aguilar-Arevalo et al., *Evidence for neutrino oscillations from the observation of $\bar{\nu}_e$ appearance in a $\bar{\nu}_\mu$ beam*, *Phys. Rev. D* **64** (2001) 112007 [[hep-ex/0104049](#)].
- [59] G. Mention, M. Fechner, T. Lasserre, T. A. Mueller, D. Lhuillier, M. Cribier et al., *The Reactor Antineutrino Anomaly*, *Phys.Rev.D* **83** (2011) [[1101.2755](#)].
- [60] S. Böser, C. Buck, C. Giunti, J. Lesgourgues, L. Ludhova, S. Mertens et al., *Status of Light Sterile Neutrino Searches*, *Prog.Part.Nucl.Phys.* **111** (2020) [[1906.01739](#)].
- [61] J. A. Formaggio, E. Figueroa-Feliciano and A. J. Anderson, *Sterile Neutrinos, Coherent Scattering and Oscillometry Measurements with Low-temperature Bolometers*, *Phys.Rev.D* **85** (2012) [[1107.3512](#)].
- [62] B. Dutta, Y. Gao, R. Mahapatra, N. Mirabolfofathi, L. E. Strigari and J. W. Walker, *Sensitivity to oscillation with a sterile fourth generation neutrino from ultra-low threshold neutrino-nucleus coherent scattering*, *Phys.Rev.D* **94** (2016) [[1511.02834](#)].
- [63] B. C. Cañas, E. A. Garcés, O. G. Miranda and A. Parada, *The reactor antineutrino anomaly and low energy threshold neutrino experiments*, *Phys.Lett.B* **776** (2018) 451 [[1708.09518](#)].

- [64] C. Blanco, D. Hooper and P. Machado, *Constraining Sterile Neutrino Interpretations of the LSND and MiniBooNE Anomalies with Coherent Neutrino Scattering Experiments*, *Phys.Rev.D* **101** (2020) [[1901.08094](#)].
- [65] O. G. Miranda, D. K. Papoulias, O. Sanders, M. Tórtola and J. W. F. Valle, *Future CEvNS experiments as probes of lepton unitarity and light-sterile neutrinos*, *Phys.Rev.D* **102** (2020) [[2008.02759](#)].
- [66] C. Hagmann and A. Bernstein, *Two-phase emission detector for measuring coherent neutrino-nucleus scattering*, *IEEE Trans.Nucl.Sci.* **51** (2004) 2151 [[nucl-ex/0411004](#)].
- [67] A. Bernstein, N. Bowden, B. L. Goldblum, P. Huber, I. Jovanovic and J. Mattingly, *Colloquium: Neutrino detectors as tools for nuclear security*, *Rev.Mod.Phys.* **92** (2020) [[1908.07113](#)].
- [68] M. Bowen and P. Huber, *Reactor neutrino applications and coherent elastic neutrino nucleus scattering*, *Phys.Rev.D* **102** (2020) [[2005.10907](#)].
- [69] CONNIE collaboration, A. Aguilar-Arevalo et al., *The CONNIE experiment*, *J. Phys. Conf. Ser.* **761** (2016) 012057 [[1608.01565](#)].
- [70] MINER collaboration, G. Agnolet et al., *Background Studies for the MINER Coherent Neutrino Scattering Reactor Experiment*, *Nucl. Instrum. Meth. A* **853** (2017) 53 [[1609.02066](#)].
- [71] J. Colaresi, J. I. Collar, T. W. Hossbach, A. R. L. Kavner, C. M. Lewis, A. E. Robinson et al., *First results from a search for coherent elastic neutrino-nucleus scattering at a reactor site*, *Phys. Rev. D* **104** (2021) 072003 [[2108.02880](#)].
- [72] J. J. Choi, *Neutrino Elastic-scattering Observation with NaI(Tl)(NEON)*, *PoS NuFact2019* (2020) 047.
- [73] ν -CLEUS collaboration, R. Strauss et al., *The ν -cleus experiment: A gram-scale fiducial-volume cryogenic detector for the first detection of coherent neutrino-nucleus scattering*, *Eur. Phys. J. C* **77** (2017) 506 [[1704.04320](#)].
- [74] ν GEN collaboration, V. Belov et al., *The ν GeN experiment at the Kalinin Nuclear Power Plant*, *JINST* **10** (2015) P12011.
- [75] RED-100 collaboration, D. Y. Akimov et al., *First ground-level laboratory test of the two-phase xenon emission detector RED-100*, *JINST* **15** (2020) P02020 [[1910.06190](#)].
- [76] RICOCHET collaboration, J. Billard et al., *Coherent Neutrino Scattering with Low Temperature Bolometers at Chooz Reactor Complex*, *J. Phys. G* **44** (2017) 105101 [[1612.09035](#)].
- [77] TEXONO collaboration, H. T. Wong, *The TEXONO research program on neutrino and astroparticle physics*, *Mod. Phys. Lett. A* **19** (2004) 1207.
- [78] G. Fernandez Moroni, J. Estrada, E. E. Paolini, G. Canelo, J. Tiffenberg and J. Molina, *Charge Coupled Devices for detection of coherent neutrino-nucleus scattering*, *Phys. Rev. D* **91** (2015) 072001 [[1405.5761](#)].
- [79] ν -CLEUS collaboration, R. Strauss et al., *Gram-scale cryogenic calorimeters for rare-event searches*, *Phys. Rev. D* **96** (2017) 022009 [[1704.04317](#)].
- [80] CONUS collaboration, H. Bonet et al., *Large-size sub-keV sensitive germanium detectors for the CONUS experiment*, *Eur. Phys. J. C* **81** (2021) 267 [[2010.11241](#)].

- [81] V. Chepel and H. Araujo, *Liquid noble gas detectors for low energy particle physics*, *JINST* **8** (2013) [1207.2292].
- [82] J. J. Choi, B. J. Park, C. Ha, K. W. Kim, S. K. Kim, Y. D. Kim et al., *Improving the light collection using a new NaI(Tl) crystal encapsulation*, *Nucl. Instrum. Meth. A* **981** (2020) 164556 [2006.02573].
- [83] A. C. Hayes and P. Vogel, *Reactor Neutrino Spectra*, *Ann.Rev.Nucl.Part.Sci.* **66** (2016) 219 [1605.02047].
- [84] P. Huber, *On the determination of anti-neutrino spectra from nuclear reactors*, *Phys. Rev. C* **84** (2011) 024617 [1106.0687].
- [85] T. A. Mueller, D. Lhuillier, M. Fallot, A. Letourneau, S. Cormon, M. Fechner et al., *Improved Predictions of Reactor Antineutrino Spectra*, *Phys.Rev.C* **83** (2011) [1101.2663].
- [86] DAYA BAY collaboration, F. P. An et al., *Improved Measurement of the Reactor Antineutrino Flux and Spectrum at Daya Bay*, *Chin. Phys. C* **41** (2017) 013002 [1607.05378].
- [87] V. Kopeikin, L. Mikaelyan and V. Sinev, *Components of anti-neutrino emission in nuclear reactor*, *Phys.Atom.Nucl.* **67** (2004) 1963 [hep-ph/0308186].
- [88] GEMMA collaboration, A. G. Beda, V. B. Brudanin, E. V. Demidova, V. G. Egorov, M. G. Gavrilov, M. V. Shirchenko et al., *First Result for Neutrino Magnetic Moment from Measurements with the GEMMA Spectrometer*, *Phys. Atom. Nucl.* **70** (2007) 1873 [0705.4576].
- [89] X. B. Ma, W. L. Zhong, L. Z. Wang, Y. X. Chen and J. Cao, *Improved calculation of the energy release in neutron-induced fission*, *Phys.Rev.C* **88** (2013) [1212.6625].
- [90] G. Heusser, *Low-radioactivity background techniques*, *Ann.Rev.Nucl.Part.Sci.* **45** (1995) 543.
- [91] G. Heusser, M. Weber, J. Hakenmüller, M. Laubenstein, M. Lindner, W. Maneschg et al., *GIOVE - A new detector setup for high sensitivity germanium spectroscopy at shallow depth*, *Eur.Phys.J.C* **75** (2015) 531 [1507.03319].
- [92] CONUS collaboration, J. Hakenmüller et al., *Neutron-induced background in the CONUS experiment*, *Eur. Phys. J. C* **79** (2019) 699 [1903.09269].
- [93] H. Bonet et al., *Full background decomposition of the CONUS experiment*, 2112.09585.
- [94] J. Lindhard and M. Scharff, *Energy Dissipation by Ions in the keV Region*, *Phys.Rev.* **124** (1961) 128.
- [95] B. J. Scholz, A. E. Chavarria, J. I. Collar, P. Privitera and A. E. Robinson, *Measurement of the low-energy quenching factor in germanium using an $^{88}\text{Y}/\text{Be}$ photoneutron source*, *Phys. Rev. D* **94** (2016) 122003 [1608.03588].
- [96] J. I. Collar, A. R. L. Kavner and C. M. Lewis, *Germanium response to sub-keV nuclear recoils: a multipronged experimental characterization*, *Phys. Rev. D* **103** (2021) 122003 [2102.10089].
- [97] P. Sorensen, *Atomic limits in the search for galactic dark matter*, *Phys. Rev. D* **91** (2015) 083509 [1412.3028].
- [98] J. Liao, H. Liu and D. Marfatia, *Coherent neutrino scattering and the Migdal effect on the quenching factor*, *Phys. Rev. D* **104** (2021) 015005 [2104.01811].
- [99] S. S. Wilks, *The Large-Sample Distribution of the Likelihood Ratio for Testing Composite Hypotheses*, *Annals Math.Statist.* **9** (1938) 60.

- [100] G. Cowan, K. Cranmer, E. Gross and O. Vitells, *Asymptotic formulae for likelihood-based tests of new physics*, *Eur.Phys.J.C* **71** (2011) 1554 [[1007.1727](#)].
- [101] L. Lista, *Practical Statistics for Particle Physicists*, in *2016 European School of High-Energy Physics*, pp. 213–258, 2017, [1609.04150](#), DOI.
- [102] R. H. Helm, *Inelastic and Elastic Scattering of 187-MeV Electrons from Selected Even-Even Nuclei*, *Phys. Rev.* **104** (1956) 1466.
- [103] S. Klein and J. Nystrand, *Exclusive vector meson production in relativistic heavy ion collisions*, *Phys.Rev.C* **60** (1999) [[hep-ph/9902259](#)].
- [104] COHERENT collaboration, D. Akimov et al., *COHERENT 2018 at the Spallation Neutron Source*, [1803.09183](#).
- [105] D. Aristizabal Sierra, J. Liao and D. Marfatia, *Impact of form factor uncertainties on interpretations of coherent elastic neutrino-nucleus scattering data*, *JHEP* **06** (2019) 141 [[1902.07398](#)].
- [106] C. Giunti and C. W. Kim, *Fundamentals of Neutrino Physics and Astrophysics*. Oxford Univ., 2007.
- [107] L. A. Mikaelyan, *Investigation of neutrino properties in experiments at nuclear reactors: Present status and prospects*, *Phys.Atom.Nucl.* **65** (2002) 1173 [[hep-ph/0210047](#)].
- [108] S. Perkins, *Tables and Graphs of Atomic Subshell and Relaxation Data Derived from the LLNL Evaluated Atomic Data Library (EADL)*, Z. Lawrence Livermore National Laboratory, 1991.
- [109] K. W. Jones and H. W. Kraner, *Stopping of 1- to 1.8-keV Ge-73 Atoms in Germanium*, *Phys. Rev. C* **4** (1971) 125.
- [110] K. W. Jones and H. W. Kraner, *Energy lost to ionization by 254-eV Ge-73 atoms stopping in Ge*, *Phys. Rev. A* **11** (1975) 1347.
- [111] Y. Messous, *Calibration of a Ge crystal with nuclear recoils for the development of a dark matter detector*, *Astropart. Phys.* **3** (1995) 361.
- [112] P. S. Barbeau, J. I. Collar and O. Tench, *Large-Mass Ultra-Low Noise Germanium Detectors: Performance and Applications in Neutrino and Astroparticle Physics*, *JCAP* **09** (2007) 009 [[nucl-ex/0701012](#)].
- [113] D. Barker and D. M. Mei, *Germanium Detector Response to Nuclear Recoils in Searching for Dark Matter*, *Astropart. Phys.* **38** (2012) 1 [[1203.4620](#)].
- [114] CONUS collaboration, H. Bonet et al., *First limits on neutrino electromagnetic properties from the CONUS experiment*, [2201.12257](#).
- [115] H. Dembinski, P. Ongmongkolkul, C. Deil, D. M. Hurtado, H. Schreiner, M. Feickert et al., *scikit-hep/iminuit: v2.0.0*, Dec., 2020. [10.5281/zenodo.4310361](#).
- [116] F. James and M. Roos, *Minuit - a system for function minimization and analysis of the parameter errors and correlations*, *Computer Physics Communications* **10** (1975) 343.
- [117] T. E. Oliphant, *Python for scientific computing*, *Computing in Science Engineering* **9** (2007) 10.
- [118] K. J. Millman and M. Aivazis, *Python for scientists and engineers*, *Computing in Science Engineering* **13** (2011) 9.

- [119] P. Virtanen et al., *SciPy 1.0: Fundamental algorithms for scientific computing in Python*, *Nature Methods* **17** (2020) 261.
- [120] J. D. Hunter, *Matplotlib: A 2d graphics environment*, *Computing in Science Engineering* **9** (2007) 90.
- [121] F. Perez and B. E. Granger, *Ipython: A system for interactive scientific computing*, *Computing in Science Engineering* **9** (2007) 21.
- [122] C. R. Harris et al., *Array programming with NumPy*, *Nature* **585** (2020) 357.
- [123] W. McKinney, *Data Structures for Statistical Computing in Python*, *Proceedings of the 9th Python in Science Conference* (2010) 56.
- [124] JupyterLab, “JupyterLab 3.0.15 documentation.” Online: <https://jupyterlab.readthedocs.io/en/stable/> (accessed 05.11.2021), 2021.
- [125] L. Dalcín, R. Paz and M. Storti, *MPI for Python*, *Journal of Parallel and Distributed Computing* **65** (2005) 1108.
- [126] L. Dalcín, R. Paz, M. Storti and J. D’Elía, *MPI for Python: Performance improvements and MPI-2 extensions*, *Journal of Parallel and Distributed Computing* **68** (2008) 655.
- [127] Y. Farzan and M. Tortola, *Neutrino oscillations and Non-Standard Interactions*, *Front.in Phys.* **6** (2018) 10 [1710.09360].
- [128] Y. Du and J.-H. Yu, *Neutrino non-standard interactions meet precision measurements of N_{eff}* , *JHEP* **05** (2021) 058 [2101.10475].
- [129] C. J. Stapleford, D. J. Väänänen, J. P. Kneller, G. C. McLaughlin and B. T. Shapiro, *Nonstandard Neutrino Interactions in Supernovae*, *Phys.Rev.D* **94** (2016) [1605.04903].
- [130] D. Aristizabal Sierra, V. De Romeri and N. Rojas, *COHERENT analysis of neutrino generalized interactions*, *Phys.Rev.D* **98** (2018) [1806.07424].
- [131] I. Bischer and W. Rodejohann, *General neutrino interactions from an effective field theory perspective*, *Nucl.Phys.B* **947** (2019) [1905.08699].
- [132] M. Hoferichter, J. Menéndez and A. Schwenk, *Coherent elastic neutrino-nucleus scattering: EFT analysis and nuclear responses*, *Phys.Rev.D* **102** (2020) [2007.08529].
- [133] K. J. Healey, A. A. Petrov and D. Zhuridov, *Nonstandard neutrino interactions and transition magnetic moments*, *Phys. Rev. D* **87** (2013) 117301 [1305.0584].
- [134] D. K. Papoulias and T. S. Kosmas, *Neutrino transition magnetic moments within the non-standard neutrino–nucleus interactions*, *Phys.Lett.B* **747** (2015) 454 [1506.05406].
- [135] A. Rohatgi, “Webplotdigitizer: Version 4.5.” Online: <https://automeris.io/WebPlotDigitizer> (accessed 26.11.2021), 2021.
- [136] XENON collaboration, E. Aprile et al., *Search for Coherent Elastic Scattering of Solar 8B Neutrinos in the XENON1T Dark Matter Experiment*, *Phys. Rev. Lett.* **126** (2021) 091301 [2012.02846].
- [137] CHARM collaboration, J. Dorenbosch et al., *Experimental Verification of the Universality of ν_e and ν_μ Coupling to the Neutral Weak Current*, *Phys. Lett. B* **180** (1986) 303.
- [138] A. Friedland, M. L. Graesser, I. M. Shoemaker and L. Vecchi, *Probing Nonstandard Standard Model Backgrounds with LHC Monojets*, *Phys. Lett. B* **714** (2012) 267 [1111.5331].

- [139] P. Coloma, I. Esteban, M. C. Gonzalez-Garcia and M. Maltoni, *Improved global fit to Non-Standard neutrino Interactions using COHERENT energy and timing data*, *JHEP* **02** (2020) 023 [[1911.09109](#)].
- [140] J. Abdallah, H. Araujo, A. Arbey, A. Ashkenazi, A. Belyaev, J. Berger et al., *Simplified Models for Dark Matter Searches at the LHC*, *Phys.Dark Univ.* **9-10** (2015) 8 [[1506.03116](#)].
- [141] D. Abercrombie, N. Akchurin, E. Akilli, J. Alcaraz Maestre, B. Allen, B. Alvarez Gonzalez et al., *Dark Matter Benchmark Models for Early LHC Run-2 Searches: Report of the ATLAS/CMS Dark Matter Forum*, *Phys.Dark Univ.* **27** (2020) [[1507.00966](#)].
- [142] A. Boveia et al., *Recommendations on presenting LHC searches for missing transverse energy signals using simplified s-channel models of dark matter*, *Phys. Dark Univ.* **27** (2020) 100365 [[1603.04156](#)].
- [143] F. Kahlhoefer, K. Schmidt-Hoberg, T. Schwetz and S. Vogl, *Implications of unitarity and gauge invariance for simplified dark matter models*, *JHEP* **02** (2016) 016 [[1510.02110](#)].
- [144] J. Ellis, M. Fairbairn and P. Tunney, *Anomaly-Free Dark Matter Models are not so Simple*, *JHEP* **08** (2017) 053 [[1704.03850](#)].
- [145] E. Morgante, *Simplified Dark Matter Models*, *Adv.High Energy Phys.* **2018** (2018) [[1804.01245](#)].
- [146] G. Arcadi, G. Busoni, T. Hugle and V. T. Tenorth, *Comparing 2HDM + Scalar and Pseudoscalar Simplified Models at LHC*, *JHEP* **06** (2020) 098 [[2001.10540](#)].
- [147] N. Vignaroli, *Leptoquarks in B-meson anomalies: simplified models and HL-LHC discovery prospects*, *Nuovo Cim. C* **43** (2020) 53 [[1912.00899](#)].
- [148] M. Bauer, P. Foldenauer and J. Jaeckel, *Hunting All the Hidden Photons*, *JHEP* **07** (2018) 094 [[1803.05466](#)].
- [149] G. Arcadi, M. D. Campos, M. Lindner, A. Masiero and F. S. Queiroz, *Dark sequential Z' portal: Collider and direct detection experiments*, *Phys. Rev. D* **97** (2018) 043009 [[1708.00890](#)].
- [150] P. B. Denton, Y. Farzan and I. M. Shoemaker, *Testing large non-standard neutrino interactions with arbitrary mediator mass after COHERENT data*, *JHEP* **07** (2018) 037 [[1804.03660](#)].
- [151] ATLAS collaboration, M. Aaboud et al., *Search for high-mass new phenomena in the dilepton final state using proton-proton collisions at $\sqrt{s} = 13$ TeV with the ATLAS detector*, *Phys. Lett. B* **761** (2016) 372 [[1607.03669](#)].
- [152] B. Batell, M. Pospelov and A. Ritz, *Exploring Portals to a Hidden Sector Through Fixed Targets*, *Phys.Rev.D* **80** (2009) [[0906.5614](#)].
- [153] J. D. Bjorken, R. Essig, P. Schuster and N. Toro, *New Fixed-Target Experiments to Search for Dark Gauge Forces*, *Phys.Rev.D* **80** (2009) [[0906.0580](#)].
- [154] S. Bilmis, I. Turan, T. M. Aliev, M. Deniz, L. Singh and H. T. Wong, *Constraints on Dark Photon from Neutrino-Electron Scattering Experiments*, *Phys.Rev.D* **92** (2015) [[1502.07763](#)].
- [155] M. Lindner, F. S. Queiroz, W. Rodejohann and X.-J. Xu, *Neutrino-electron scattering: general constraints on Z' and dark photon models*, *JHEP* **05** (2018) 098 [[1803.00060](#)].
- [156] BABAR collaboration, J. P. Lees et al., *Search for a Dark Photon in e^+e^- Collisions at BaBar*, *Phys. Rev. Lett.* **113** (2014) 201801 [[1406.2980](#)].

- [157] BABAR collaboration, J. P. Lees et al., *Search for Invisible Decays of a Dark Photon Produced in e^+e^- Collisions at BaBar*, *Phys. Rev. Lett.* **119** (2017) 131804 [[1702.03327](#)].
- [158] LHCb collaboration, R. Aaij et al., *Search for Dark Photons Produced in 13 TeV pp Collisions*, *Phys. Rev. Lett.* **120** (2018) 061801 [[1710.02867](#)].
- [159] P. Ilten, Y. Soreq, M. Williams and W. Xue, *Serendipity in dark photon searches*, *JHEP* **06** (2018) 004 [[1801.04847](#)].
- [160] R. Harnik, J. Kopp and P. A. N. Machado, *Exploring ν Signals in Dark Matter Detectors*, *JCAP* **07** (2012) 026 [[1202.6073](#)].
- [161] O. G. Miranda, D. K. Papoulias, G. Sanchez Garcia, O. Sanders, M. Tórtola and J. W. F. Valle, *Implications of the first detection of coherent elastic neutrino-nucleus scattering (CEvNS) with Liquid Argon*, *JHEP* **05** (2020) 130 [[2003.12050](#)].
- [162] N. F. Bell, G. Busoni and I. W. Sanderson, *Self-consistent Dark Matter Simplified Models with an s -channel scalar mediator*, *JCAP* **03** (2017) 015 [[1612.03475](#)].
- [163] M. Cirelli, E. Del Nobile and P. Panci, *Tools for model-independent bounds in direct dark matter searches*, *JCAP* **10** (2013) 019 [[1307.5955](#)].
- [164] A. Bonhomme et al., *Direct measurement of the ionization quenching factor of nuclear recoils in germanium in the keV energy range*, [2202.03754](#).
- [165] M. Blennow, E. Fernandez-Martinez, T. Ota and S. Rosauero-Alcaraz, *Physics potential of the ESS ν SB*, *Eur. Phys. J. C* **80** (2020) 190 [[1912.04309](#)].
- [166] D. Baxter, J. I. Collar, P. Coloma, C. E. Dahl, I. Esteban, P. Ferrario et al., *Coherent Elastic Neutrino-Nucleus Scattering at the European Spallation Source*, *JHEP* **02** (2020) 123 [[1911.00762](#)].
- [167] J. B. Dent, B. Dutta, S. Liao, J. L. Newstead, L. E. Strigari and J. W. Walker, *Accelerator and reactor complementarity in coherent neutrino-nucleus scattering*, *Phys.Rev.D* **97** (2018) [[1711.03521](#)].
- [168] M. Lindner, W. Rodejohann and X.-J. Xu, *Neutrino Parameters from Reactor and Accelerator Neutrino Experiments*, *Phys.Rev.D* **97** (2018) [[1709.10252](#)].
- [169] C. Bellenghi, D. Chiesa, L. Di Noto, M. Pallavicini, E. Previtali and M. Vignati, *Coherent elastic nuclear scattering of ^{51}Cr neutrinos*, *Eur. Phys. J. C* **79** (2019) 727 [[1905.10611](#)].
- [170] M. Cadeddu, F. Dordei, C. Giunti, K. A. Kouzakov, E. Picciau and A. I. Studenikin, *Potentialities of a low-energy detector based on ^4He evaporation to observe atomic effects in coherent neutrino scattering and physics perspectives*, *Phys. Rev. D* **100** (2019) 073014 [[1907.03302](#)].
- [171] M. Abdullah, D. Aristizabal Sierra, B. Dutta and L. E. Strigari, *Coherent Elastic Neutrino-Nucleus Scattering with directional detectors*, *Phys.Rev.D* **102** (2020) [[2003.11510](#)].
- [172] D. Aristizabal Sierra, B. Dutta, D. Kim, D. Snowden-Ifft and L. E. Strigari, *Coherent elastic neutrino-nucleus scattering with the $\nu\text{BDX-DRIFT}$ directional detector at next generation neutrino facilities*, *Phys. Rev. D* **104** (2021) 033004 [[2103.10857](#)].
- [173] O. Tomalak, P. Machado, V. Pandey and R. Plestid, *Flavor-dependent radiative corrections in coherent elastic neutrino-nucleus scattering*, *JHEP* **02** (2021) 097 [[2011.05960](#)].